UNIVERSITY OF CALIFORNIA

Los Angeles

Highly Sensitive Electronic Skins

A dissertation submitted in partial satisfaction of the

requirements for the degree Doctor of Philosophy

in Material Science and Engineering

by

Yun-Chiao Huang

2018

ABSTRACT OF THE DISSERTATION

Highly Sensitive Electronic Skins

by

Yun-Chiao Huang

Doctor of Philosophy in Materials Science and Engineering

University of California, Los Angeles, 2018

Professor Yu Huang, Chair

Electronic skins (E-skins) with sensory capabilities mimicking human-skin or beyond are essential for wearable healthcare monitoring devices, robotic technologies, human-machine interface (HMI) and artificial intelligence (AI). The ability to rapidly detect small pressure variation represents an important function of E-skins. Here we report a new design of pressure-sensing E-skins by integrating a unique conductive microstructured air-gap (CMAG) gate with two-dimensional (2D) semiconductor transistors to achieve unprecedented combination of ultrahigh sensitivity, rapid response, low power consumption and long-term stability. We first show that the CMAG can be used to create the capacitor-based E-skins with a highest sensitivity

up to 770.4 kPa^{-1} (*vs.* ~ 4.5 kPa^{-1} reported previously). By employing the CMAGs as pressure sensitive gate for 2D MoS_2 transistors, we show that the pressure sensitivity can be further amplified to achieve a highest value of ~ 2.61 × 10^7 kPa^{-1} (*vs.* the previous record of 192 kPa^{-1}). Along with ultrafast response (< 0.1 ms), lower power consumption (~ 9 pW−270 nW), low minimum pressure detection (< 0.05 Pa) and excellent stability, our device delivers an overall performance well above the existing pressure-sensing E-skins, enabling highly sensitive static pressure mapping, real-time human pulse wave measurements, E-skin microphone for speech pattern recognition, and remote pressure monitoring.

The dissertation of Yun-Chiao Huang is approved.

Jaime Marian

Xiangfeng Duan

Yu Huang, Committee Chair

University of California, Los Angeles

2018

Deliciated to my beloved parents and family

for their unconditional love, support, and encouragement

致我的父母與家人

感謝他們對我的愛、支持與鼓勵

Table of Contents

List of Figures

Supplementary Materials

Acknowledgements

It has been a great privilege to be a doctoral student at University of California, Los Angeles. I am grateful for the opportunities to learn from the faculty and students in wide range of fields from materials science, chemistry, electrical engineering, mechanical engineering, to computer science. My Ph.D. journey during these five years will be one of the important periods in my life. I particularly thank those who have inspired, encouraged, and supported me during these years.

Firstly, I would like to express my sincere gratitude to my research advisors, Prof. Xiangfeng Duan and Prof. Yu Huang, for their invaluable guidance, inspiration, and support by sharing with me their profound knowledge and helping me to think outside of the box. I am also grateful for the freedom they have given me to explore my own adventure in research fields. Their life philosophy and positive attitude at work have motivated me to be a better person. I could not have imagined having a better advisor and mentor for my Ph.D. study. Besides my research advisors, I would like to thank the rest of my thesis committee, Prof. Dwight C. Streit and Prof. Jaime Marian, for their encouragement and insightful comments.

My sincere thanks also goes to Prof. Jenn-Ming Yang (UCLA), Prof. Fu-Hsing Lu (NCHU), Prof. Fuh-Sheng Shieu (NCHU), and Prof. Ko-Wei Lin (NCHU), who have supported me and given me valuable advices throughout my Ph.D. journey, and Prof. Steven Nutt (USC), who encouraged me to explore different research fields and helped me to make my transition from USC to UCLA smoothly. I would like to thank Mr. Wannien Lin for his generosity in funding the Wannien fellowship, which supported my education at UCLA.

I also thank all my labmates from departments of Materials Science and Engineering and Chemistry and Biochemistry, especially for Dr. Yuan Liu, Dr. Qiyuan He, Dr. Hung-Chieh Chen, Dr. Hao Wu, Dr. Chen Wang, Mr. Chao Ma, Mr. Cheng-Yi Lin, Mr. Sungjoon Lee, Dr. Chuancheng Jia, Dr. Chen Peng, Mr. Jian Guo, Dr. Mufan Li, Dr. Zhaoyang Lin, Mr. Yiliu Wang, Mr. Peiqi Wang, Mr. Guangyan Zhong, Dr. Rui Cheng, Dr. Shan Jiang, Dr. Chain Lee, Mr. Sen Yang, Dr. Yongjia Li, Dr. Zipeng Zhao, Dr. Enbo Zhu, Dr. Yu Chen, and Dr. Dehui Li, for the stimulating discussions, the supportive help, and all the fun we have had in the last five years. All of them make my Ph.D. life more delightful.

Last but not least, I would like to thank my family and friends for supporting me throughout my Ph.D. journey in the U.S. They have selflessly encouraged me to explore new directions in life and sought my own destiny. This journey would not have been possible if not for them, and I dedicate this milestone to them!

Biography

Yun-Chiao Huang received her B.S. degree in Materials Science and Engineering from National Chung Hsing University (Taiwan), and two master's degrees in Electrical Engineering and Materials Science from University of Southern California. In 2013, she joined Prof. Yu Huang's lab to conduct research on highly sensitive electronic skins for pressure sensing and their applications under Prof. Xiangfeng Duan's and Prof. Yu Huang's guidance. She will receive her Ph.D. degree in Materials Science and Engineering from University of California, Los Angeles in 2018. She was awarded UCLA Fellowship from 2013 to 2014, UCLA WANNIEN Fellowship from 2014 to 2017, and UCLA Dissertation Year Fellowship (DYF) from 2017 to 2018. She has one U.S. patent pending and one co-author paper in *Nature*. Her research interests include soft electronics, flexible/wearable electronic skins, and the related applications (*i.e.*, healthcare monitoring, pressure mapping for touch devices, remote pressure monitoring, and E-skin microphone for speech pattern recognition).

Chapter 1: Introduction

Electronic skin (E-skin) is an artificial skin with human-like sensory capabilities, especially for pressure sensing that transduces an applied force into an electrical signal, which has attracted significant attention due to the increasing demand for flexible electronic devices such as wearable healthcare monitoring, human-machine interface (HMI), robotic technologies, microelectromechanical systems (MEMS), microphones, hearing aids[1-11], *etc*. The future E-skins should not just mimic the real human skin, but provide functions or performance beyond the natural skin to satisfy many crucial application requirements, *i.e.*, higher sensitivity especially in low pressure regime (< 100 Pa, suitable for lower vibrational force; < 10 kPa, approximate to gentle touch), along with other desirable features including faster response in millisecond, lower power consumption, long-term air stability and robustness for wearable electronic devices[12-16]. Recently, E-skins for pressure sensing have been developed different physical transduction mechanisms, including piezoresistivity, capacitance, transistor, piezoelectricity, optics, triboelectricity, *etc.*[4,6-8,13,17-27]; among these, piezoresistivity, capacitance, and transistor have been widely investigated and used in the pressure sensors and related applications.

Generally, the mechanism of piezoresistive sensors is to monitor the change of resistance in order to obtain the corresponding applied pressure; these sensors are broadly used due to their simple design and readout mechanism[28]. Typically, the piezoresistive E-skins are able to sensitively respond to the pressure variations by changing the contact resistance between two conductive materials or the conductive path in the elastic conductive composites. For example, sandwiching ultrathin gold nanowire-impregnated tissue paper between two thin polydimethylsiloxane sheets can realize the piezoresistive pressure sensors, which exhibit high

pressure sensitivity ~ 1.14 kPa^{-1}, fast response ~ 17 ms, and minimum pressure detection of 13 Pa[17]. The stretchable piezoresistive pressure sensors, by integrating the conductive microstructured elastomer with the counter electrode, show relatively linear pressure response with higher sensitivity ~ 4.88 kPa^{-1} when pressure is less than 6 kPa[28]. In addition, the piezoresistive E-skins constructed of the elastic polymer embedded with different types of conductive fillets, such as carbon nanotubes, metallic particles, graphene, etc.[18-21], have been widely fabricated due to their low cost and simple preparation.

Besides piezoresistive pressure sensors, capacitive and transistor-based E-skins for pressure sensing have attracted considerable interest recently. The capacitor-based E-skins feature simple device design, easy readout, excellent stability, and low power consumption[4,22,23], while the transistor-based E-skins offer signal amplification, higher sensitivity, and lower power consumption[7,8]. Notably, by integrating the capacitive structure as the pressure sensitive gate with the gate-absent transistors, the transistor-based pressure sensors can be created showing the enhanced pressure sensitivity and faster response. Recent studies have demonstrated exciting developments in both types of E-skins. For examples, using compressible dielectrics or air gaps to overcome the less compressible and viscoelastic behavior of rubbers has greatly enhanced the sensitivity and the response time of capacitor-based E-skins[9,29]. Integrating carbon nanotube or organic transistors with pressure sensitive rubber (PSR) or microstructured dielectrics has led to significantly improved performance[6,7,13,24,25].

The mechanisms of these pressure sensors are usually governed by the compressibility of the material contacted directly with the applied force. In general, the greater the compressibility of the materials exhibits, the higher the sensitivity and the signal-to-noise ratio (SNR) of the pressure

sensors can deliver. The compressibility is also related to the Young's modulus of the elastomers. For example, under the same stress, the elastomers with low Young's modulus tend to deform more, leading to higher sensitivity compared to that with higher Young's modulus. However, the elastomers with low Young's modulus exhibit greater viscoelastic behavior that limits the response speed. As a result, it is of considerable challenge to achieve both high sensitivity and fast response at the same time. Using the silicone elastomer as a dielectric in the compressible capacitors for pressure sensing has realized a sensitivity of 2.3×10^{-4} kPa^{-1} with the pressure sensing range from 50 kPa to 1 MPa, which is too large for mimicking the human-like sensing capabilities such as gentle manipulation of items[4]. The development of capacitive pressure sensors by using microstructured elastic dielectric has shown dramatic improvements of the sensitivity (~ 0.55 kPa^{-1}) and response/relaxation times (<< 1 s) compared to that with the unstructured elastic dielectric (sensitivity ~ 0.02 kPa^{-1} and response/relaxation times > 10 s) or the polymer foam (sensitivity ~ 5×10^{-4} kPa^{-1} and the response/relaxation times >> 20 s)[9,22]. Nevertheless, the sensitivity is still limited by (i) the less compressible dielectrics and (ii) the large thickness of the elastomers (~ 10−500 μm)[7,9,22,30-32] that contributes the denominator in the normalized capacitance change, leading to lower sensitivity and lower SNR. In addition, the response time is restricted by the natural viscoelastic behaviour of rubber. Therefore, the main challenge is to form a "real air-gap" device that is not limited by the thick and less compressible elastomers. To this end, a flexible aluminium/polyimide composite electrode has been invented as an air-gap capacitive pressure sensor with a sensitivity of ~ 4.5 kPa^{-1} when pressure is in the range of ~ 0−3 kPa[8], which represents the highest sensitivity achieved in capacitance-based E-skins to date[4,7-9,22,23,29,31-36].

To further enhance the sensitivity, the transistor-based E-skins with an impressive sensitivity of 8.4 kPa^{-1} and fast response time of < 10 ms has been demonstrated by integrating

organic thin film transistors (OTFTs) with the elastic microstructured dielectrics[7]. Recently, other transistor-based pressure sensors have also been proposed by using the flexible suspended gate on OTFTs to create the unstructured air gaps, delivering an ultrahigh sensitivity of 192 kPa^{-1} and rapid response time of < 10 ms[8]. However, the sensitivity, SNR, and response time of these pressure sensors are still limited by the lack of the "true" microstructured air gaps and inherent viscoelastic behaviour of rubbers. Moreover, the performance of the organic transistors usually degrades in air[37-39]; the relatively low mobility is not ideal for large amplification and the devices often require large operation voltage (*e.g.*, up to 200 V)[7,8,39], which is not desirable for practical applications in E-skins.

To improve the sensitivity, response and air stability, and reduce the power consumption of the pressure sensing E-skins, herein we report a new design of the conductive microstructured air gaps (CMAGs) to replace the current microstructured dielectrics, in which the overall capacitance is only determined by the highly compressible microstructured air gaps with little contribution from the less compressible thick elastomers, realizing a "true" microstructured air-gap device with an ultrahigh sensitivity and fast response. Taking a step further, we integrate the CMAGs with 2D semiconductor materials (*e.g.*, MoS_2 and WSe_2) to realize flexible CMAG-2D semiconductor E-skins with further enhanced pressure sensing performance. Our capacitor-based E-skins deliver an impressive sensitivity of up to 770.4 kPa^{-1}, far exceeding the highest sensitivity (~ 4.5 kPa^{-1}) achieved previously in capacitive pressure sensors[4,7-9,22,23,29,31-36]. Furthermore, the CMAG-MoS_2 E-skins exhibit an unprecedented sensitivity (~ 2.61×10^7 kPa^{-1} *vs.* 192 kPa^{-1} from the transistor-based pressure sensors reported previously[8]). Additionally, our CMAG-MoS_2 E-skin exhibits many other favourable features, including ultrafast response time (< 0.1 ms *vs.* ~ 10 ms reported previously[7,8]), lower power consumption (9 pW−270 nW), minimum pressure detection

(< 0.05 Pa *vs.* ~ 0.5 Pa reported before[8]), excellent air stability and robustness. With these outstanding pressure-sensing capabilities, our E-skins allow highly sensitive static pressure mapping, real-time human pulse wave measurement, E-skin microphone for speech pattern recognition, and remote pressure monitoring.

References

1 Hattori, Y. *et al.* Multifunctional skin-like electronics for quantitative, clinical monitoring of cutaneous wound healing. *Advanced healthcare materials* **3**, 1597-1607 (2014).

2 Kang, D. *et al.* Ultrasensitive mechanical crack-based sensor inspired by the spider sensory system. *Nature* **516**, 222-226 (2014).

3 Kim, D.-H. *et al.* Epidermal electronics. *Science* **333**, 838-843 (2011).

4 Lipomi, D. J. *et al.* Skin-like pressure and strain sensors based on transparent elastic films of carbon nanotubes. *Nature Nanotech.* **6**, 788-792 (2011).

5 Tee, B. C.-K. *et al.* A skin-inspired organic digital mechanoreceptor. *Science* **350**, 313-316 (2015).

6 Yeom, C. *et al.* Large-Area Compliant Tactile Sensors Using Printed Carbon Nanotube Active-Matrix Backplanes. *Adv. Mater.* **27**, 1561-1566 (2015).

7 Schwartz, G. *et al.* Flexible polymer transistors with high pressure sensitivity for application in electronic skin and health monitoring. *Nat. Commun.* **4**, 1859 (2013).

8 Zang, Y. *et al.* Flexible suspended gate organic thin-film transistors for ultra-sensitive pressure detection. *Nature communications* **6**, 6269 (2015).

9 Mannsfeld, S. C. *et al.* Highly sensitive flexible pressure sensors with microstructured rubber dielectric layers. *Nature materials* **9**, 859 (2010).

10 Lee, S. *et al.* A transparent bending-insensitive pressure sensor. *Nat Nanotechnol* **11**, 472-478 (2016).

11 Graz, I. *et al.* Flexible ferroelectret field-effect transistor for large-area sensor skins and microphones. *Applied physics letters* **89**, 073501 (2006).

12 Dellon, E. S., Mourey, R. & Dellon, A. L. Human pressure perception values for constant and moving one-and two-point discrimination. *Plast. Reconstr. Surg.* **90**, 112-117 (1992).

13 Kaltenbrunner, M. *et al.* An ultra-lightweight design for imperceptible plastic electronics. *Nature* **499**, 458 (2013).

14 Pan, L. *et al.* An ultra-sensitive resistive pressure sensor based on hollow-sphere microstructure induced elasticity in conducting polymer film. *Nature communications* **5**, 3002 (2014).

15 Pang, C. *et al.* A flexible and highly sensitive strain-gauge sensor using reversible interlocking of nanofibres. *Nature materials* **11**, 795 (2012).

16 Chae, S. H. *et al.* Transferred wrinkled Al2O3 for highly stretchable and transparent graphene–carbon nanotube transistors. *Nat Mater* **12**, 403-409 (2013).

17 Gong, S. *et al.* A wearable and highly sensitive pressure sensor with ultrathin gold nanowires. *Nature communications* **5**, 3132 (2014).

18 Maheshwari, V. & Saraf, R. F. High-resolution thin-film device to sense texture by touch. *Science* **312**, 1501-1504 (2006).

19 Chun, K.-Y. *et al.* Highly conductive, printable and stretchable composite films of carbon nanotubes and silver. *Nature nanotechnology* **5**, 853 (2010).

20 Yan, C. *et al.* Highly stretchable piezoresistive graphene–nanocellulose nanopaper for strain sensors. *Advanced materials* **26**, 2022-2027 (2014).

21 Wang, Y. *et al.* Wearable and highly sensitive graphene strain sensors for human motion monitoring. *Advanced Functional Materials* **24**, 4666-4670 (2014).

22 Metzger, C. *et al.* Flexible-foam-based capacitive sensor arrays for object detection at low cost. *Appl. Phys. Lett.* **92**, 013506 (2008).

23 Lee, J. *et al.* Conductive Fiber-Based Ultrasensitive Textile Pressure Sensor for Wearable Electronics. *Adv. Mater.* **27**, 2433-2439 (2015).

24 Sekitani, T. *et al.* Organic nonvolatile memory transistors for flexible sensor arrays. *Science* **326**, 1516-1519 (2009).

25 Takei, K. *et al.* Nanowire active-matrix circuitry for low-voltage macroscale artificial skin. *Nature materials* **9**, 821 (2010).

26 Yun, S. *et al.* Polymer-waveguide-based flexible tactile sensor array for dynamic response. *Advanced Materials* **26**, 4474-4480 (2014).

27 Wang, S., Lin, L. & Wang, Z. Triboelectric nanogenerators as self-powered active sensors. *Nano Energy* **11**, 436-462 (2015)

28 Choong, C. L. *et al.* Highly stretchable resistive pressure sensors using a conductive elastomeric composite on a micropyramid array. *Advanced materials* **26**, 3451-3458 (2014).

29 Lee, H.-K., Chang, S.-I. & Yoon, E. A flexible polymer tactile sensor: fabrication and modular expandability for large area deployment. *J. Microelectromech. Syst.* **15**, 1681-1686 (2006).

30 Lee, B.-Y., Kim, J., Kim, H., Kim, C. & Lee, S.-D. Low-cost flexible pressure sensor based on dielectric elastomer film with micro-pores. *Sens. Actuator A-Phys.* **240**, 103-109 (2016).

31 Lei, K. F., Lee, K.-F. & Lee, M.-Y. A flexible PDMS capacitive tactile sensor with adjustable measurement range for plantar pressure measurement. *Microsys. Technol.* **20**, 1351-1358 (2014).

32 Zhang, B. *et al.* Dual functional transparent film for proximity and pressure sensing. *Nano Res.* **7**, 1488-1496 (2014).

33 Park, S. *et al.* Stretchable Energy-Harvesting Tactile Electronic Skin Capable of Differentiating Multiple Mechanical Stimuli Modes. *Adv. Mater.* **26**, 7324-7332 (2014).

34 Boutry, C. M. *et al.* A Sensitive and Biodegradable Pressure Sensor Array for Cardiovascular Monitoring. *Adv. Mater.* **27**, 6954-6961 (2015).

35 Pang, C. *et al.* Highly Skin-Conformal Microhairy Sensor for Pulse Signal Amplification. *Adv. Mater.* **27**, 634-640 (2015).

36 Tee, B. C. K. *et al.* Tunable flexible pressure sensors using microstructured elastomer geometries for intuitive electronics. *Adv. Funct. Mater.* **24**, 5427-5434 (2014).

37 Pannemann, C., Diekmann, T. & Hilleringmann, U. Degradation of organic field-effect transistors made of pentacene. *J. Mater. Res.* **19**, 1999-2002 (2004).

38 Sirringhaus, H. Reliability of Organic Field-Effect Transistors. *Adv. Mater.* **21**, 3859-3873 (2009).

39 Manunza, I. & Bonfiglio, A. Pressure sensing using a completely flexible organic transistor. *Biosens. Bioelectron.* **22**, 2775-2779 (2007).

Chapter 2: Conductive microstructured air gaps (CMAGs)

A. Introduction of the CMAGs

The development of capacitor-based E-skins for pressure sensing by using microstructured elastomers has shown dramatic improvements recently. However, it is still of considerable challenge to achieve both high pressure sensitivity and fast response at the same time, because the microstructured dielectrics are still fabricated by rubbers, which have relatively small deformation upon compression compared to air and inhere serious viscoelastic behavior leading to slower and non-linear pressure response. In order to overcome these challenges, herein we have innovated a unique design of the conductive microstructured air gaps (CMAGs) to replace the current microstructured elastomers, in which the overall capacitance is only determined by the highly compressible microstructured air gaps with little contribution from the less compressible thick elastomers, realizing a "true" microstructured air-gap device with an ultrahigh sensitivity and fast response. Furthermore, we evaluate and compare the normalized capacitance change in our CMAG device *vs.* the conventional air-gap device in response of physical deformation under the applied pressure by using highly simplified parallel plate capacitor model and simulations. Finally, we discuss the sensing performance of CMAG E-skins *vs.* resistor-based E-skins if the cracks occur during the bending or cyclic loading conditions.

B. CMAG fabrication

The detailed fabrication processes are described in Section G. Methods and Fig. 2-1. The CMAG consists of a regular array of microstructured pyramids fabricated by casting

polydimethylsiloxane (PDMS) in a silicon mold followed by direct deposition of Au as the conductive layer on the microstructured pyramids. The sizes (heights and widths) and periodicity of pyramids can be readily tailored for specific pressure sensing requirements. The flexible CMAG capacitive E-skins were assembled by laminating the continuous conductive microstructured PDMS pyramid array (supported on PET substrate) with a flexible PET substrate coated with the layers of Cr/Au thin film (20 nm/80 nm) as the bottom electrodes and Al_2O_3 dielectric (30 nm) (Fig. 2-2a-b), which allows large-area and scalable fabrication of a matrix array for pressure sensing devices. To further enhance the pressure sensing performance, we fabricated the transistor-based E-skins by integrating the CMAGs with 2D MoS_2 and WSe_2 transistors (Fig. 2-2c). The scanning electron microscope (SEM) image of the conductive microstructured PDMS shows a highly uniform array of micro-pyramids (Fig. 2-2d).

C. The design and evaluation of the CMAGs: *Parallel plate capacitor model*

First, a highly simplified parallel plate capacitor model is used to evaluate and compare the normalized capacitance change in our CMAG device *vs.* the conventional air-gap device in response of physical deformation under applied pressure. We assume that the device area of the parallel plate capacitor model would not change under the applied pressure in order to simply the evaluation. The conventional microstructured air-gap devices have a conductive layer on the flat backside of the microstructured PDMS (Fig. 2-3a). With this design, the total capacitance is approximately contributed by two capacitors in series: the elastomer-based capacitor (which has relatively small change upon compression) and the air-gap capacitor that responds sensitively to the mechanical deformation.

The capacitance change can thus be expressed as:

$$\Delta C_{Conventional} = C - C_o = \frac{A\varepsilon_{Air}\varepsilon_{PDMS}}{d'_{Air}\varepsilon_{PDMS} + d'_{PDMS}\varepsilon_{Air}} - \frac{A\varepsilon_{Air}\varepsilon_{PDMS}}{d_{Air}\varepsilon_{PDMS} + d_{PDMS}\varepsilon_{Air}} = \frac{A\varepsilon_{Air}\varepsilon_{PDMS}(\varepsilon_{PDMS}\Delta d_{Air} + \varepsilon_{Air}\Delta d_{PDMS})}{(d_{Air}\varepsilon_{PDMS} + d_{PDMS}\varepsilon_{Air})(d'_{Air}\varepsilon_{PDMS} + d'_{PDMS}\varepsilon_{Air})}$$

(2-1)

, where A is the device area; ε_{Air} (= 1.0) and ε_{PDMS} (~ 3.0) are the dielectric constant of air and PDMS, respectively; Δd_{Air} (= d_{Air} - d'_{Air}) and Δd_{PDMS} (= d_{PDMS} - d'_{PDMS}) are the thickness change of air and PDMS, correspondingly; d_{Air}, d'_{Air}, d_{PDMS} and d'_{PDMS} are denoted as the initial and final thickness of air and PDMS, individually. Then, the normalized capacitance change can be expressed as:

$$\frac{\Delta C_{Conventional}}{C_o} = \frac{\varepsilon_{PDMS}\Delta d_{Air} + \varepsilon_{Air}\Delta d_{PDMS}}{d'_{Air}\varepsilon_{PDMS} + d'_{PDMS}\varepsilon_{Air}} \sim \frac{\varepsilon_{PDMS}\Delta d_{Air}}{d'_{Air}\varepsilon_{PDMS} + d'_{PDMS}\varepsilon_{Air}} \qquad (2\text{-}2)$$

Typically, the Young's modulus of PDMS is usually ~ 0.57−3.7 MPa[1,2]. Under the applied pressure less than 10 kPa, d'_{PDMS} approximately equals to d_{PDMS}, resulting in $\varepsilon_{Air}\,\Delta d_{PDMS} << \varepsilon_{PDMS}\,\Delta d_{Air}$. Therefore, we can obtain the equation of the normalized capacitance change for the conventional E-skin as shown in the last term in equation (2-2).

The normalized capacitance change, sensitivity, and SNR of this structure are governed by the thickness change of air gap (Δd_{Air}) and the final thickness of the elastomer and air dielectrics (d'_{PDMS} and d'_{Air}). Typically, the thickness of air gaps is around 2−3 μm and the thickness of elastomer is about 10−500 μm[3-6]. As a result, d'_{PDMS} (~ d_{PDMS}) in equation (2-2) dominates the pressure sensing performance. Therefore, in this design, the thinner the elastomer dielectric is, the higher the sensitivity and SNR of the E-skin can achieve. However, it is of considerable challenge

to aggressively shrink the thickness of the elastomer while maintaining the microstructured air gaps, which has thus limited the normalized capacitance change and sensitivity of the devices. In addition, although the conventional microstructured air-gap devices have shown that the response/relaxation times is faster than those without the microstructured elastomer dielectrics, they still inherit the viscoelastic behavior of elastomers, which limits their response/relaxation times (typically ~ 10−1,000 ms regime)[3,4].

To address these challenges, we propose to use the CMAGs (Fig. 2-3a) as a pressure sensitive dielectric. With this design, the capacitance is only approximately contributed by the air-gap component, so the change of the capacitance under the applied pressure is determined by the deformation of the microstructured air gaps without considering the effects of the elastomer dielectrics, which leads to greatly enhanced sensitivity, normalized capacitance change, and SNR. The capacitance change can be expresses as:

$$\Delta C_{Conductive} = C - C_o = \frac{A\varepsilon_{Air}}{d'_{Air}} - \frac{A\varepsilon_{Air}}{d_{Air}} = \frac{A\varepsilon_{Air}(d_{Air} - d'_{Air})}{d'_{Air}d_{Air}} = \frac{A\varepsilon_{Air}\Delta d_{Air}}{d'_{Air}d_{Air}} \qquad (2\text{-}3)$$

Thus, the normalized capacitance change for the CMAG devices can be expresses as:

$$\frac{\Delta C_{Conductive}}{C_o} = \frac{\Delta d_{Air}}{d'_{Air}} \qquad (2\text{-}4)$$

In the compression state, the higher the compression pressure applies, the less the final thickness of air (d'_{Air}) is. As a result, $\Delta C_{Conductive}/C_o$ is increasingly larger than $\Delta C_{Conventional}/C_o$ as the applied pressure increases. Under the specific applied pressure, when d'_{Air} approaches 0, leading to

$$\Delta C_{Conductive} >> \Delta C_{Conventional} \qquad (2\text{-}5)$$

As a result, when the applied pressure increases, $\Delta C_{Conductive}$ becomes dramatically larger than $\Delta C_{Conventional}$, resulting that the CMAG devices exhibit higher normalized capacitance change and higher sensitivity compared to that of conventional devices under the same pressure load.

D. The design and evaluation of the CMAGs: *Simulations of CMAG devices vs. conventional microstructured devices*

To further investigate the merits of CMAGs, we have simulated the potential gradient and the capacitance change of our CMAG devices upon deformation and compared with the conventional microstructured devices by constructing the microstructured pyramid model (the height, width and periodicity of the pyramid are ~ 3.6, 6.0, and 13.6 μm, respectively) under the compression (Fig. 2-3a-c). The energy stored in the capacitive pressure sensor can be expressed as following:

$$U = \frac{1}{2} C V^2 \qquad (2\text{-}6)$$

, where C and V represent capacitance and electric potential, respectively. If the energy is stored in the electric field, then the energy density in a dielectric medium is expressed as

$$U = \frac{1}{2} \varepsilon E^2 \qquad (2\text{-}7)$$

, where ε and E are the permittivity of the medium and electric field, respectively. From equation (2-6) and (2-7), we can obtain the equation as following:

$$C = \varepsilon \frac{E^2}{V^2} \qquad (2\text{-}8)$$

As a result, C is proportional to the gradient of electric potential, ∇V, because of $E = -\nabla V$. In order to clearly show the simulation results, the top assembly with the CMAGs is flipped to the bottom with an applied voltage at 1.5 V on the CMAGs, and the electrode on the bottom assembly is flipped to the top and grounded (but we do not show it here) (Fig. 2-3b-c). Notably, our CMAG devices show dramatic potential gradient changes (*e.g.*, higher capacitance due to $C \propto \nabla V$) not only on the top of the pyramids but also the rest areas when compared to that of the conventional device (Fig. 2-3b); the capacitance distribution of our CMAG devices is also significantly higher than that of the conventional structure under the same deformation (Fig. 2-3c). As the deformation increases (*i.e.*, the applied pressure increases), $\Delta C_{Conductive}/C_o$ is increasingly larger than $\Delta C_{Conventional}/C_o$ (Fig. 2-4). Both analyses from highly simplified parallel plate capacitor model and simulations show that our CMAG devices have great advantages in normalized capacitance change and the corresponding pressures sensitivity compared to that of conventional microstructured devices under the same pressure load.

E. Crack effect on the sensing performance of CMAG E-skins *vs.* resistor-based E-skins

It should be noted that repeated deformation of the micro-pyramids could lead to crack formation. We chose Au as the conductive metal thin film for its excellent ductility and flexibility

to mitigate the extensive crack formation[7-10]. Additionally, comparing with the E-skins using the conductive microstructures (*i.e.*, CNTs, nanoscale crack junctions, nanowires, *etc.*) as resistive pressure sensors[7,11], the performance of our CMAG E-skins is less sensitive to the cracks even in the extreme case with complete crack and discontinuous conductive films.

The mechanism of the resistor-based sensors such as crack-based sensors is governed by the conductivity change due to the change in contact area of the conductive structures or fillets under the applied pressure. For example, the mechanism of a 20 nm-thick Pt on the elastomer as a crack-based sensors is attributed to the disconnection-reconnection process of zip-like nanoscale crack junctions under vibration or strain[7]. This study also mentioned that their crack mechanism can only apply to the stiff metal such as Pt but not ductile metals (*e.g.*, Au), which does not form the straight cracks and remain fully connected while film was stretched[7-10]. Indeed, our study of the Au thin film on PDMS also supports this conclusion.

It is important to note the capacitive sensor mechanism is not sensitive to the cracks (when compared with resistor-based sensors) even in the extreme case with complete crack and discontinuous conductive films (Fig. 2-5a). To this end, we have evaluated a highly simplified crack model using the parallel plate capacitors, where the top Au film (which is discontinuous with a complete crack in the middle) is applied with a bias of 1.5 V (only left portion is biased and there is no direct bias on the right portion due to the crack), the total capacitance of the device consists of C_{CMAG1} in parallel with two capacitors (C_{CMAG2} and C_{crack} in series) (Fig. 2-5b). The total capacitance can be expressed as

$$C_{total} = C_{CMAG1} + \frac{C_{CMAG2} C_{crack}}{C_{CMAG2} + C_{crack}} \qquad (2\text{-}9)$$

, where C_{CMAG1} and C_{CMAG2} are the capacitance of the left and right portions of the CMAG capacitors, correspondingly. C_{crack} is the capacitance of the crack between the top Au electrodes.

Considering typical crack width ~ 5–30 nm, and the height of the microstructured air gaps ~ 3–5 μm), leading to $C_{crack} >> C_{CMAG2}$, the equation (2-9) can be simplified as the following:

$$C_{total} \simeq C_{CMAG1} + \frac{C_{CMAG2} C_{crack}}{C_{crack}} \simeq C_{CMAG1} + C_{CMAG2} \qquad (2\text{-}10)$$

Therefore, the total capacitance of the device with a small crack roughly equals to that without the crack. This analysis suggests that the cracks do not contribute significantly to the high sensitivity in our capacitive sensing mechanism. Together, the mechanism of our CMAG-based pressure sensor is determined by the capacitance change due to the deformation (compression) of microstructured air gaps but not the conductivity change while applying the pressure load. A few small cracks within the CMAG devices are not expected to contribute significantly to the sensing performance.

F. Summary

The unique design of our CMAGs can overcome the challenges of conventional microstructured devices, low pressure sensitivity and slow response, because the capacitance of CMAG devices is only approximately contributed by the microstructured air-gap component without unwanted contribution from the elastomers, which enables elastic deformation of air leading to greatly enhanced sensitivity, higher normalized capacitance change, and higher SNR. Moreover, both analyses from the highly simplified parallel plate capacitor model and the

simulations show that the design of CMAGs has considerable advantages over the conventional design (*e.g.*, higher $\Delta C/C_o$ and higher sensitivity under the same applied pressure). This "true" microstructured air-gap design minimizes the impact by the unwanted viscoelastic behavior of elastomers, which could also promise faster response speed, along with greatly enhanced sensitivity. Furthermore, we observed that a few small cracks within the CMAG devices are not expected to contribute significantly to the sensing performance based on our analysis; the mechanism of our CMAG E-skins is determined by the capacitance change due to the deformation of the microstructured air gaps but not the mechanism of the resistor-based pressure sensors (*e.g.*, the conductivity change while applying the pressure loads).

In summary, the concept of CMAGs shows greater pressure sensing performances (*i.e.*, higher pressure sensitivity, higher SNR, and relatively crack-insensitive sensing performance) over that of conventional microstructured devices. Importantly, the unique design of CMAGs can create capacitor- or transistor-based E-skins for specific pressure sensing applications.

G. Methods

CMAG fabrication. The CMAGs were created by casting PDMS in a pre-fabricated silicon (Si) mold (Fig. 2-1). The microstructured Si mold was made from <100> Si wafers with 300-nm-thick SiO_2. The Si substrate was first patterned using photolithography to produce a square array of open windows with exposed SiO_2. The exposed SiO_2 was stripped using buffered hydrofluoric acid (BOE), and the remaining SiO_2 was used as a mask for potassium hydroxide (KOH) etching, followed by octadecyltrichlorosilane (OTS) surface treatment to facilitate the subsequent release

of PDMS cast from the Si mold. A 1:5 mixture of curing agent to PDMS elastomer (Sylgard 184, Dow Corning) was prepared, diluted with hexane (1:10 PDMS mixture to hexane), and then stirred overnight. The diluted solution filtered by 0.2-μm-PTFE-membrane filter, which is easy to fill into the microstructured mold, and then degassed. A 125-μm-thick PET (MELINEX ST505 5.0 mil) was plasma-treated for 10 min and placed on top of the degassed PDMS with the mold in vacuum, followed by baking at a temperature around 120 ºC for 4 hours. The microstructured PDMS pyramids supported by PET substrate was peeled off from the Si mold. A conductive metal thin film (Au: 70−100 nm) layer was then deposited on microstructured PDMS by electron beam (e-beam) evaporation. A rotating sample holder was used during the e-beam process to ensure a continuous conductive layer covering the entire microstructured surface.

Device characterization. SEM images of the conductive microstructured pyramids were taken using TESCAN VEGA3.

H. Figures

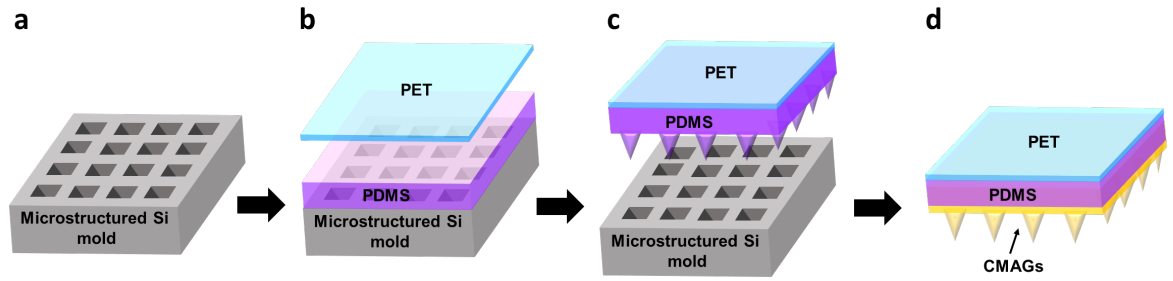

Figure 2-1 | Fabrication processes of the CMAGs. **(a)** Si mold with inverse microstructured pyramids was patterned using photolithography, the SiO_2 uncovered by photoresist was stripped using buffered hydrofluoric acid (BOE), and the remaining SiO_2 was used as a mask for KOH etching. **(b)** A dilute mixture of polydimethylsiloxane (PDMS), curing agent, and hexane was drop cast onto an octadecyltrichlorosilane (OTS)-treated Si mold, and then polyethylene terephthalate (PET) supporting layer was placed on top of the PDMS followed by curing at ~ 120 ^{o}C for 4 hours. **(c)** After curing, the flexible PDMS/PET was peeled off the mold. **(d)** Au layers were deposited on the microstructured pyramids by e-beam evaporation. A rotating sample holder was used during the e-beam process to ensure a continuous conductive layer across the entire microstructured surface.

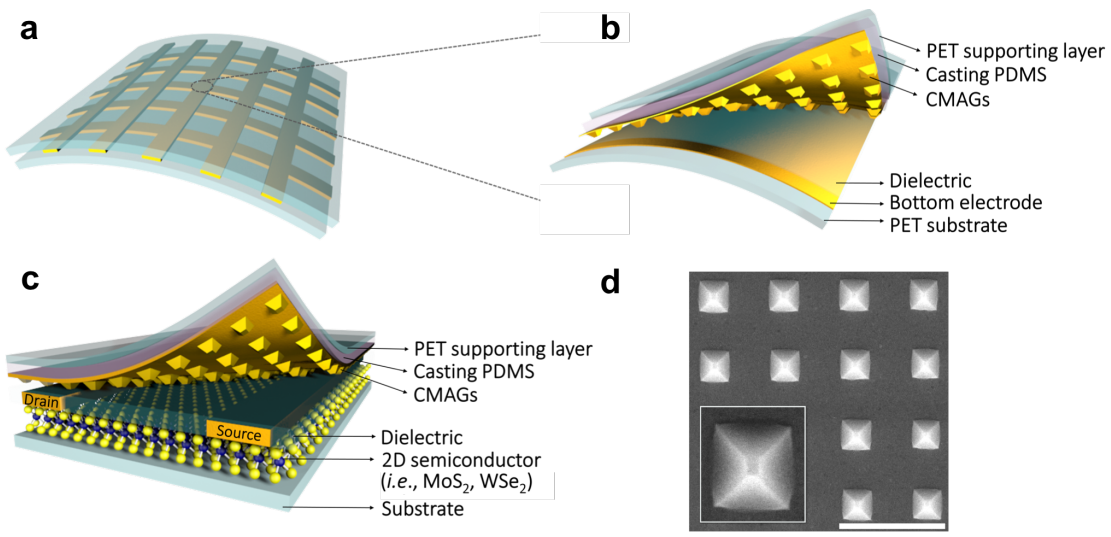

Figure 2-2 | Capacitor- and transistor-based E-skins with the CMAGs. (a) Schematic illustration of a 5 × 5 capacitive pressure sensor array with the CMAGs. **(b)** Zoomed-in view of the device structure from **a**. The E-skin is made by laminating the top stack (the CMAGs on PET substrate) and the bottom stack (dielectric/bottom electrode/PET substrate) together. **(c)** Schematic illustration of the CMAG-2D semiconductor E-skin including two assemblies. The top contains the CMAGs on PET substrate and the bottom is composed of the dielectric layers, source and drain electrodes, and 2D semiconducting channel (*e.g.*, MoS_2 and WSe_2) on the substrate. **(d)** SEM images of top-view conductive microstructured pyramids with an inset showing a zoomed-in image. The height, width, and periodicity of the conductive pyramid are ~ 3.6, 6.0, and 13.6 μm, respectively. The scale bar is denoted as 20 μm.

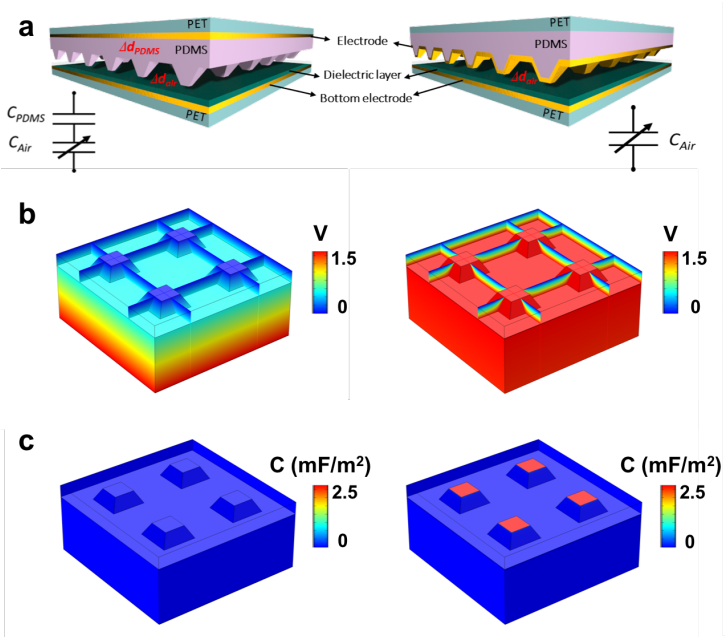

Figure 2-3 | Flexible CMAG capacitor-based E-skins. Schematic illustrations of **(a)** the conventional capacitive pressure sensor with the microstructured elastic dielectric (the conductive electrode is deposited on the flat backside of the microstructured PDMS) and its approximately equivalent circuit (left), and our capacitor-based E-skins with the CMAGs (the conductive electrode layer is coated on the side of the microstructured pyramids) and its approximately equivalent circuit (right). Simulations of **(b)** electric potential and **(c)** unit capacitance distributions from the conventional capacitive pressure sensor (left) and our CMAG capacitor-based E-skin (right) when the deformation is ~ 40 %, correspondingly.

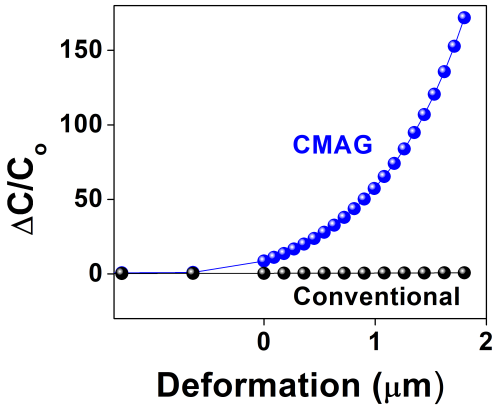

Figure 2-4 | Simulation comparisons of the normalized capacitance change from the conventional and the CMAG devices corresponding to the microstructured air gap deformation. The microstructured air gap deformation increases as the applied pressure increases. When the microstructured air gap deformation < 0, $\Delta C/C_o$ is contributed by an additional unstructured air gap formed between the top of the conductive pyramid and the bottom dielectric due to the slightly curvature of the flexible substrate, that happens frequently in the real situation, as also observed in previous studies[3].

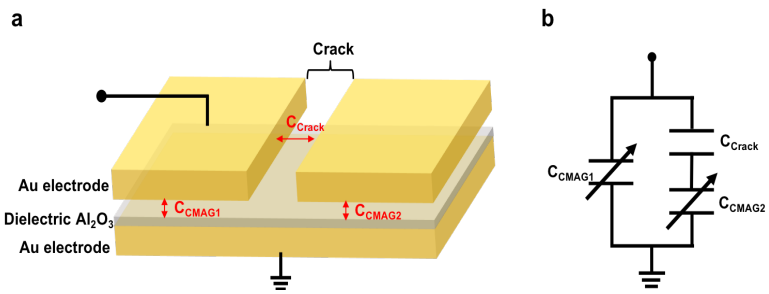

Figure 2-5 | The complete crack model caused by the discontinuous conductive films constructed by using the simplified parallel plate capacitor model. (a) The top Au electrode (150 nm x 150 nm x 80 nm) with the 10 nm-wide crack in the middle, where the left portion was applied a bias at 1.5 V with no bias applied on the right portion. The bottom assembly including the 30 nm-thick Al_2O_3 dielectric and 100 nm-thick bottom Au electrode, which is grounded. **(b)** The equivalent circuit diagram from **a** including one capacitor (C_{CMAG1}) in parallel with other two capacitors (C_{CMAG2} and C_{crack} in series).

References

1 Tee, B. C. K. *et al.* Tunable flexible pressure sensors using microstructured elastomer geometries for intuitive electronics. *Adv. Funct. Mater.* **24**, 5427-5434 (2014).

2 Wang, Y. *et al.* Wearable and highly sensitive graphene strain sensors for human motion monitoring. *Advanced Functional Materials* **24**, 4666-4670 (2014).

3 Schwartz, G. *et al.* Flexible polymer transistors with high pressure sensitivity for application in electronic skin and health monitoring. *Nat. Commun.* **4**, 1859 (2013).

4 Mannsfeld, S. C. *et al.* Highly sensitive flexible pressure sensors with microstructured rubber dielectric layers. *Nature materials* **9**, 859 (2010).

5 Metzger, C. *et al.* Flexible-foam-based capacitive sensor arrays for object detection at low cost. *Appl. Phys. Lett.* **92**, 013506 (2008).

6 Zhang, B. *et al.* Dual functional transparent film for proximity and pressure sensing. *Nano Res.* **7**, 1488-1496 (2014).

7 Kang, D. *et al.* Ultrasensitive mechanical crack-based sensor inspired by the spider sensory system. *Nature* **516**, 222-226 (2014).

8 Lacour, S. P., Wagner, S., Huang, Z. & Suo, Z. Stretchable gold conductors on elastomeric substrates. *Applied physics letters* **82**, 2404-2406 (2003).

9 Lacour, S. P., Jones, J., Wagner, S., Li, T. & Suo, Z. Stretchable interconnects for elastic electronic surfaces. *Proceedings of the IEEE* **93**, 1459-1467 (2005).

10 Graz, I. M., Cotton, D. P. & Lacour, S. P. Extended cyclic uniaxial loading of stretchable gold thin-films on elastomeric substrates. *Applied Physics Letters* **94**, 071902 (2009).

11 Chou, H.-H. *et al.* A chameleon-inspired stretchable electronic skin with interactive colour changing controlled by tactile sensing. *Nat. Commun.* **6**, 8011 (2015).

Chapter 3: Flexible CMAG capacitor-based E-skins for pressure sensing

A. Introduction of flexible capacitor-based E-skins for pressure sensing

The mechanism of the capacitive pressure sensors can be described by a parallel plate capacitor model and the capacitance can be expressed as following,

$$C = \frac{\varepsilon_o \varepsilon_r A}{d} \qquad (3\text{-}1)$$

, where ε_o and ε_r are the vacuum permittivity and dielectric constant, respectively; A is the the area of overlap of the two plates; d is the distance between two parallel plates. Generally, the capacitor-based pressure sensors are able to measure the applied pressure by monitoring the capacitance variations due to the change in the contacting area of the capacitor (A) or the distance between two parallel palates (d) under the applied force. With special design of the dielectrics (*e.g.*, different microstructures of the dielectrics), the dielectric constant of the capacitors (ε_r) can also be changed under the applied pressure[1,2]. As a result, the capacitive pressure sensors are able to measure the variations of the capacitance to obtain the corresponding pressure. For example, the mechanism of the traditional capacitor-based E-skins, by sandwiching the unstructured rubber dielectric between two parallel electrodes, is generally governed by the compressibility of the dielectrics (*e.g.*, the change in the distance between the parallel plate electrodes). As a result, the greater the compressibility of the dielectric materials exhibits, the higher the sensitivity and the signal-to-noise ratio (SNR) of the pressure sensors can deliver. Although rubbers dielectrics are able to deform under the applied pressure, the compressibility of the rubbers are still limited by their intrinsic properties (*e.g.*, Young's modulus), leading to relatively small deformation. Moreover,

rubbers have serious viscoelastic behavior, resulting slower response time and non-linear relation between pressure and signals.

In order to enhance the pressure sensitivity and shorten the response time, the capacitive pressure sensors integrating with the microstructured dielectrics have been invented, in which the microstrcutred air gaps within the rubber dielectrics enable the elastic deformation of air, allowing the devices to deform sensitively and respond faster under the external force. Nevertheless, the microstrcutred air gaps are still fabricated by rubbers; the sensitivity is still limited by the less compressible rubber dielectrics and the large thickness of the elastomers (~ 10−500 μm)[1-6] that contributes the denominator in the normalized capacitance change in equation 2-2, leading to lower sensitivity and lower SNR (please see the detail information in Section C. The design and evaluation of the CMAGs: *Parallel plate capacitor model*, Chapter 2). In addition, the natural viscoelastic behavior of rubbers leads to slower response.

To overcome these challenges, herein we present the CMAG structure to realize the "real microstructured air gaps" devices, allowing the elastic deformation of the microstructured air gaps without the unwanted viscoelastic behavior of rubbers. With the unique CMAGs, our capacitive E-skins show record-high pressure sensitivity, turnability (*e.g.*, pressure range, sensitivity, SNR, tunable linear or non-linear response, *etc.*), excellent stability and robustness.

B. Pressure sensing performance of flexible CMAG capacitor-based E-skins

The sensitivity of capacitive pressure sensors is defined as $S = \delta(\Delta C/C_o)/\delta P$, where ΔC (= $C - C_o$) is the relative change in capacitance; C and C_o are the capacitance of the sensor with and

without pressure load, respectively; P is the applied pressure. To evaluate the pressure sensitivity of our devices, we have measured the capacitance change under different pressure. The normalized capacitance change ($\Delta C/C_o$) of our devices can reach up to ~ 217 at P ~ 1.5 kPa (Fig. 3-1a), which is about 35 times higher than that of recent reported capacitance-based E-skin[7]. Importantly, the device exhibits an extraordinary sensitivity up to ~ 330 kPa^{-1} (Fig. 3-1a)**,** which is considerably higher than those achieved in recent reports: 0.005 kPa^{-1} (ref. 8); 0.21 kPa^{-1} (ref. 9); 0.55 kPa^{-1} (ref. 1); 0.55−0.58 kPa^{-1} (ref. 10); 1.5 kPa^{-1} (ref. 11). With such high sensitivity, the device can respond to the lightweight substances such as tiny pieces of paper (the pressure of a single piece of paper corresponds to 0.76 Pa). The measured capacitance changes with increasing pieces of paper show highly reproducible results even at ultralow pressure regime (< 8 Pa when 10 pieces of paper are loaded) (Fig. 3-1b). The corresponding sensitivity at ultralow pressure regime can reach up to ~ 36.6 kPa^{-1} (Fig. 3-1b), along with the minimum detectable pressure of 0.76 Pa, which outperforms similar types of pressure sensors reported to date[1,2,4-14].

Interestingly, there are two capacitance saturations located at ~ 0.09 and ~ 1 kPa of this device with increasing pressure, resulting in two minimum derivatives of $\Delta C/C_o$ (*i.e.*, the minimum pressure sensitivities) (Fig. 3-1a). Overall, when the top assembly is placed on the bottom assembly, there is usually an additional thin layer of unstructured air gap between the CMAGs and the bottom assembly due to slight curvature of the flexible substrate (Fig. 2-4), as also observed previously[2]. Therefore, as we apply increasing pressure, this unstructured air gap is first compressed, leading to rapidly increasing capacitance; when the unstructured air gap is nearly completely compressed (~6–8 Pa), the $\Delta C/C_o$ reaches first saturation (blue area in Fig. 3-1a, and Fig. 3-1b), leading to decreasing sensitivity; with further increasing the applied pressure to deform the microstructured

air gaps, $\Delta C/C_o$ rapidly increases again due to the deformation of the CMAGs, and then slows down to reach the second saturation (~ 1 kPa) when the CMAG is nearly completely deformed (orange area in Fig. 3-1a), since after that $\Delta C/C_o$ is mostly dominated by the deformation of the relatively rigid elastomer at the base of the pyramids, leading to lower sensitivity. Moreover, a moderately high sensitivity of 44.3 kPa^{-1} was achieved in a relatively broader pressure sensing range (~ 0−5 kPa) by changing the geometry and the spacing of the conductive pyramids, with linear relation between $\Delta C/C_o$ and the corresponding pressure (Fig. 3-2).

C. Tunability of the pressure sensing performance

Generally, varied sensitivities in different pressure regimes are required for specific sensing applications, so the tunable sensing performance is essential but challenging[2,7,13]. There are several parameters in our CMAG design that could affect the capacitance response to the applied pressure, such as the geometry and the spatial arrangement of the conductive pyramids (*e.g.*, the size of pyramids and periodicity, respectively), Young's modulus of the supporting layer and the substrate, the volume fraction of air within the CMAGs, *etc*. Indeed, the normalized capacitance change, sensitivity, SNR, the pressure response (linear or non-linear), and the pressure sensing range can be readily tailored for specific applications by adjusting these parameters. First, we observed that the geometry and the spatial arrangement of the conductive pyramids could considerably affect the sensing performance. Pyramid #1 (height 3.6 μm, bottom width 6.0 μm, top width 0.9 μm, periodicity 13.6 μm) with smaller conductive pyramids and smaller periodicity exhibits higher normalized capacitance change and higher sensitivity but narrower pressure

sensing range compared to Pyramid #2 (height 12 μm, bottom width 20 μm, top width 3 μm, periodicity 100 μm) with larger conductive pyramids and wider periodicity (Fig. 3-3a-b). Pyramid #1 exhibits higher $\Delta C/C_o$ and pressure sensitivity comparing to that of Pyramid #2 under the same pressure load due to more conductive pyramids touching the bottom assembly per unit area in Pyramid #1 rather than in Pyramid #2 (Fig. 3-3c).

Moreover, we also investigated the effect of the Young's modulus of the supporting layers on the sensing performance. From the classical stress-strain curve, the lower Young's modulus of the material exhibits, the larger deformation is under the same stress. Therefore, the supporting layer with lower Young's modulus leads to higher normalized capacitance change and higher sensitivity compared to that with higher Young's modulus. To highlight the effect of Young's modulus, we have investigated the sensitivity of our CMAG devices with and without PET supporting layer. As expected, the one without PET (exhibiting lower Young's modulus) is much easier to deform, leading to a record-high sensitivity up to 770.4 kPa^{-1} (average sensitivity ~ 205.4 kPa^{-1}) (Fig. 3-3d), which is more than 170 times higher than that of the recently reported capacitance-based E-skin[7]. In these ways, we can readily change the pressure sensing range, sensitivity and the normalized capacitance change by applying different Young's modulus of the supporting layer or the substrates (*e.g.*, PDMS/PET, PET, *etc.*), volume fraction of air gaps, geometry and spatial arrangement of the conductive pyramids to satisfy the specific pressure sensing applications.

D. The mechanical behaviors of the CMAG E-skins

We have further investigated the sensing performance of our CMAG E-skin upon the cyclic loading tests. In general, the pressure range and maximum pressure that our CMAG devices can endure are governed by the geometry and the spatial arrangement of the conductive pyramids. The CMAG devices show highly stable performance under repeatedly cyclic loading when pressure is less than their maximum endured pressure. Our CMAG-based pressure sensor is particularly designed for lower pressure range < 3 kPa and special applications such as pulse wave or sound wave detection. The cyclic loading test of the flexible CMAG-based E-skin under different pressure loads shows that the device is trustable and stable when pressure < 3.1 kPa (Fig. 3-4a), with reliable performance > 10,000 loading cycles at relatively large load ~ 2.58 kPa (Fig. 3-5). Furthermore, by applying high frequency sound wave testing, our E-skin is also stable for millions of cyclic loading in the sound pressure range. When pressure is above a certain critical value (~ 3 kPa), the pyramids are unable to deform elastically (*i.e.*, the conductive pyramids cannot fully recover after applying higher pressure) (Fig. 3-4b-d), the device becomes less reliable. Nonetheless, such upper limit could certainly be tailored by using a certain pressure reducing mechanism if we need to detect higher pressure regime (*e.g.*, using thicker PI or PET supporting layers with relatively large Young's modulus).

The flexible E-skins constructed on PET are also highly stable against repeated bending cycles up to 3,000 cycles while it was bent on a curve surface with the bending radius ~ 32.5 mm, which is similar to the radius of human wrist (Fig. 3-6a). After the cyclic bending test, only few conductive pyramids show the cracks occurring at the bottom edge of the conductive pyramids (Fig. 3-6b-d), demonstrating our CMAGs devices are stable for the bending tests. Importantly,

even if a few small cracks occur during the bending or cyclic loading, the performance of the capacitor-based CMAG E-skins would not be significantly affected (pleases see the detail information in Section E. Crack effect on the sensing performance of CMAG E-skins *vs.* resistor-based E-skins, Chapter 2). Moreover, we have considered impact of convex and concave bending of the CMAGs on the pressure sensing performance. For the convex bending (Fig. 3-7a), C_o slightly decreases with decreasing bending radius, since the spacing between each pyramid becomes wider but the height of pyramid remains similar, which causes less contacting areas of top of the pyramids and the bottom dielectric per unit area, leading to lower C_o. For the concave bending (Fig. 3-7b), C_o slightly increases with decreasing bending radius since the narrow spacing between each pyramid results in more contacting areas between the top and the bottom assemblies per unit area, leading to higher C_o. However, the response to such bending radius is rather small ($\Delta C/C_o \sim$ 0.05-0.42 for radius of curvature 1.35 to 7.60 cm) when compared to the pressure response ($\Delta C/C_o \sim$ 0.35-220 for the pressure range of 86 Pa to 1.5 kPa) (Fig. 3-7a-b). Therefore, the slight flex would not significantly affect the pressure response when the pressure is above 200 Pa. In addition, for typical operation where the flex curvature is kept constant (as the baseline reference), it would not affect the response to smaller pressure signal either.

E. Summary

Our flexible CMAG capacitor-based E-skins for pressure sensing deliver an impressive sensitivity up to 770.4 kPa^{-1} (*vs.* ~ 4.5 kPa^{-1} achieved previously in capacitive pressure sensors[7]) with the minimum detectable pressure of 0.76 Pa, which outperforms similar types of pressure sensors reported to date[1,2,4-14]. Moreover, a moderately high sensitivity of 44.3 kPa^{-1} can also be

achieved in a relatively broader pressure sensing range (~ 0−5 kPa) with linear relation between $\Delta C/C_o$ and the corresponding pressure. We also discuss the mechanical behaviours of the flexible CMAG capacitive sensors (*e.g.*, failure mechanism by cyclic loading test with constant and various pressure loads, influence of flexing on sensor response, bending stability tests, and crack analysis), which show that the CMAG capacitive E-skins are highly stable under repeatedly cyclic loading when pressure is less than their maximum endured pressure and the slight flex would not significantly affect the pressure response if the pressure is above 200 Pa. Notably, even if the cracks occur during the bending or cyclic loading conditions, the sensing performance of our devices would not be affected significantly based on our crack analysis.

F. Methods

Device fabrication. The single pixel of the flexible CMAG device was fabricated by integrating the top assembly (CMAG with or without 125-μm PET supporting substrate) with the bottom assembly (30-nm-thick Al_2O_3 dielectric/80-nm-thick Au/20-nm-thick Cr/125 μm-thick PET); the sensing area is from 1–10 mm^2, depending on the application purposes. In addition, a flexible 5 × 5 capacitance-based E-skin array was assembled by orthogonally laminating 5 conductive microstructured PDMS strips (~ 2.5 mm wide, supported on PET supporting layer) on 5 parallel electrodes strip (~ 2.5 mm wide, covered by 30-nm-thick Al_2O_3 dielectric) on PET substrate. The parallel electrodes were deposited by e-beam evaporation of Cr/Au (20 nm/80 nm), and Al_2O_3 dielectric was deposited by atomic layer deposition (ALD). The total area of array is 2.5 × 2.5 cm^2 and the area of each pixel is ~ 6 mm^2.

Device characterization. Capacitance measurements were taken using the Agilent E4980A LCR meter (at 1 MHz frequency, oscillator's voltage level at 1.5 V_{rms} without DC bias) under ambient conditions. The capacitance response can also be measured at lower frequency and V_{rms} (100 mV), indicating our device is sensitive even in the smaller voltage level (Fig. 3-8). Pressure was applied by loading various weights on the E-skin. Cyclic loading tests of flexible capacitive E-skin under different increasing pressure loads from 0.52-4.04 kPa and constant pressure load at 2.58 kPa on a flat surface at 1 V_{rms} and 1 kHz, respectively. Bending stability tests of flexible capacitance-based E-skin responding to a load 430 Pa was done while the device was placed on a curve surface with the bending radius ~ 32.5 mm. Capacitance response corresponding to different bending radius was measured by recording the capacitance while our device was bent with different bending radii from 1.35 to 7.60 cm.

G. Figures

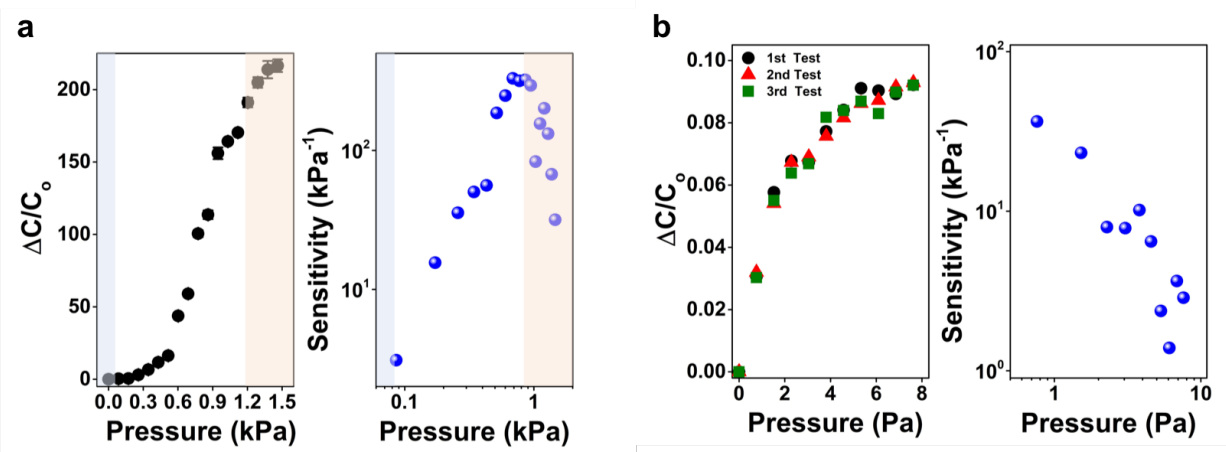

Figure 3-1 | Flexible CMAG capacitor-based E-skins. (a) The normalized capacitance change and the corresponding sensitivity as a function of varying pressure up to ~ 1.5 kPa, including two saturations (blue area: first saturation; orange area: second saturation). **(b)** The normalized capacitance change and the sensitivity of the device in the ultralow pressure regime < 8 Pa. The height, width and periodicity of the conductive pyramid are ~ 3.6, 6.0, and 13.6 μm, respectively.

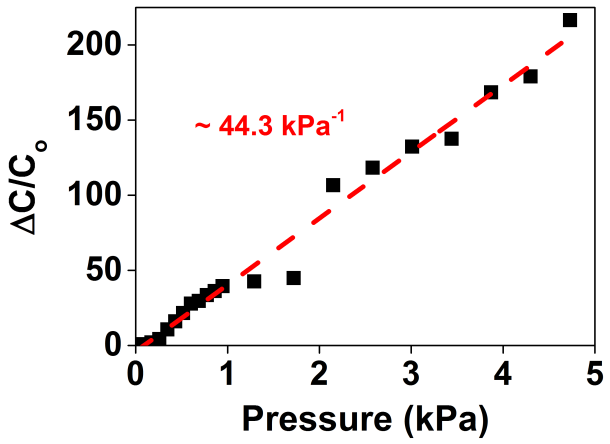

Figure 3-2 | Pressure response of the flexible CMAG capacitor-based E-skin. The height, width, and periodicity of the conductive pyramids are 12, 20, and 100 μm, respectively. Our device exhibits linear response with increasing pressure, showing a sensitivity ~ 44.3 kPa^{-1} in the pressure range of 0-5 kPa.

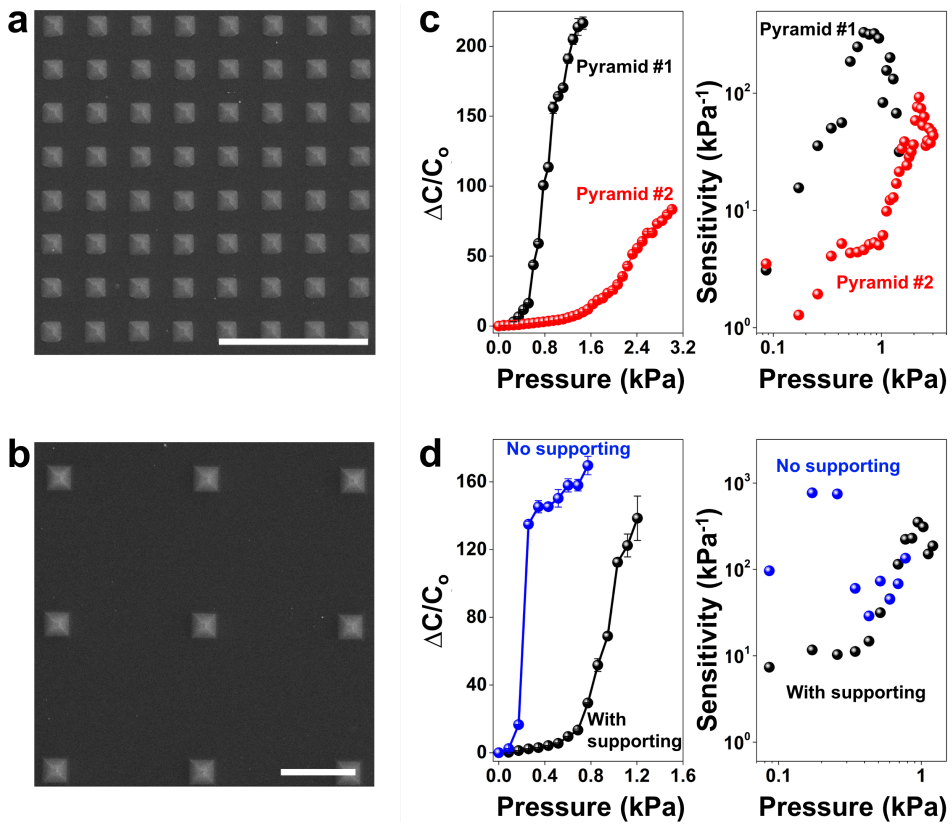

Figure 3-3 | Tunability of the CMAG capacitor-based E-skin. (a,b) Top-view SEM images of two conductive pyramids: Pyramid #1 (height 3.6 μm, bottom width 6.0 μm, top width 0.9 μm, periodicity 13.6 μm), and Pyramid #2 in **b** (height 12 μm, bottom width 20 μm, top width 3 μm, periodicity 100 μm). The scale bars represent 50 μm. (**c**) The normalized capacitance change and the sensitivity of the E-skins with different pyramid sizes and periodicities. The normalized capacitance change, sensitivity, and pressure sensing range can be readily tuned by changing the pyramid size and the periodicity. **(d)** Normalized capacitance change and the sensitivity of the E-skin made of the CMAGs with and without PET supporting layer. The CMAGs without PET are much softer and more easily deformed, leading to a higher sensitivity.

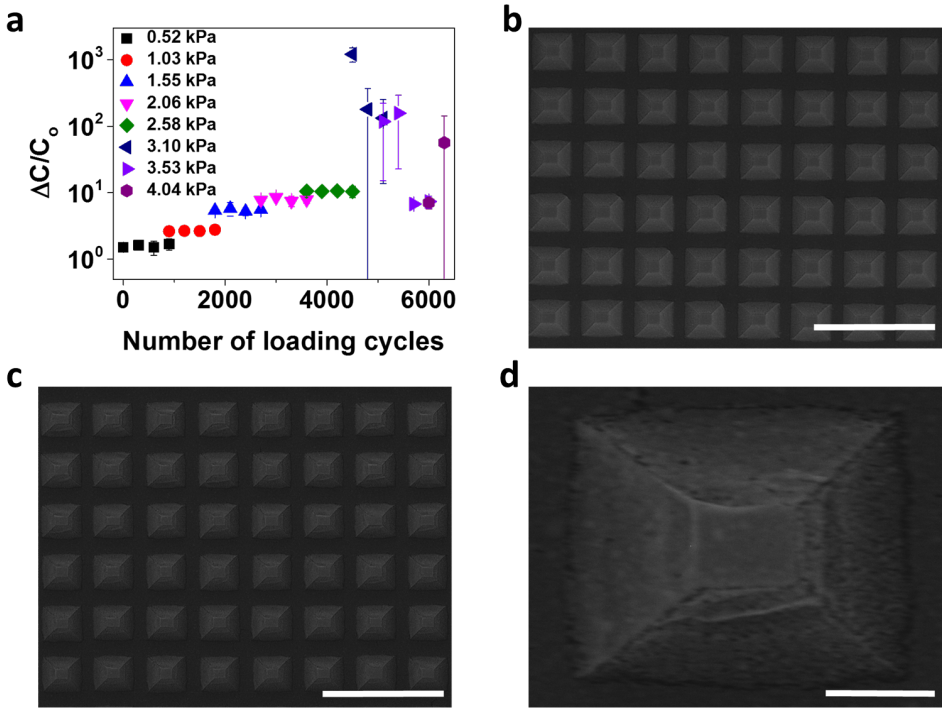

Figure 3-4 | Cyclic loading-unloading tests under different pressure loads. (a) Normalized capacitance change of the CMAGs (pyramid: height 3.7 μm, width 7.5 μm, periodicity 8.9 μm) *vs.* the number of loading cycles under different pressure levels from 0.52−4.04 kPa. SEM images of top-view conductive pyramids **(b)** before and **(c)** after loading cycles. **(d)** The zoom-in image from **c** shows the deformed conductive pyramids. The scale bars in **b**, **c** and **d** are denoted as 20 μm, 20 μm, and 2 μm, respectively.

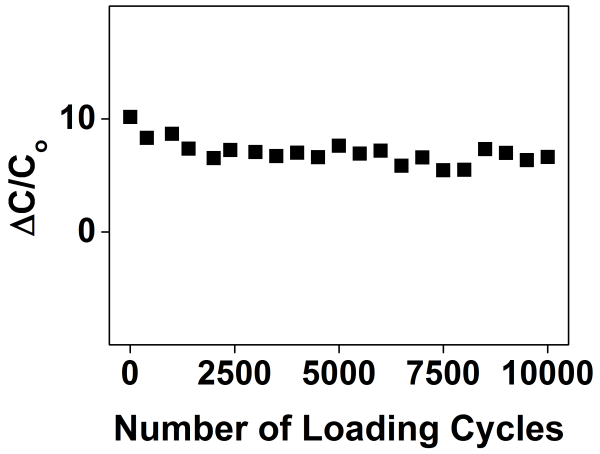

Figure 3-5 | Stability test of the flexible capacitive E-skin responding to a relatively large load of 2.58 kPa for over 10,000 loading-unloading cycles (operation voltage of 1 V_{rms}, 1 kHz).

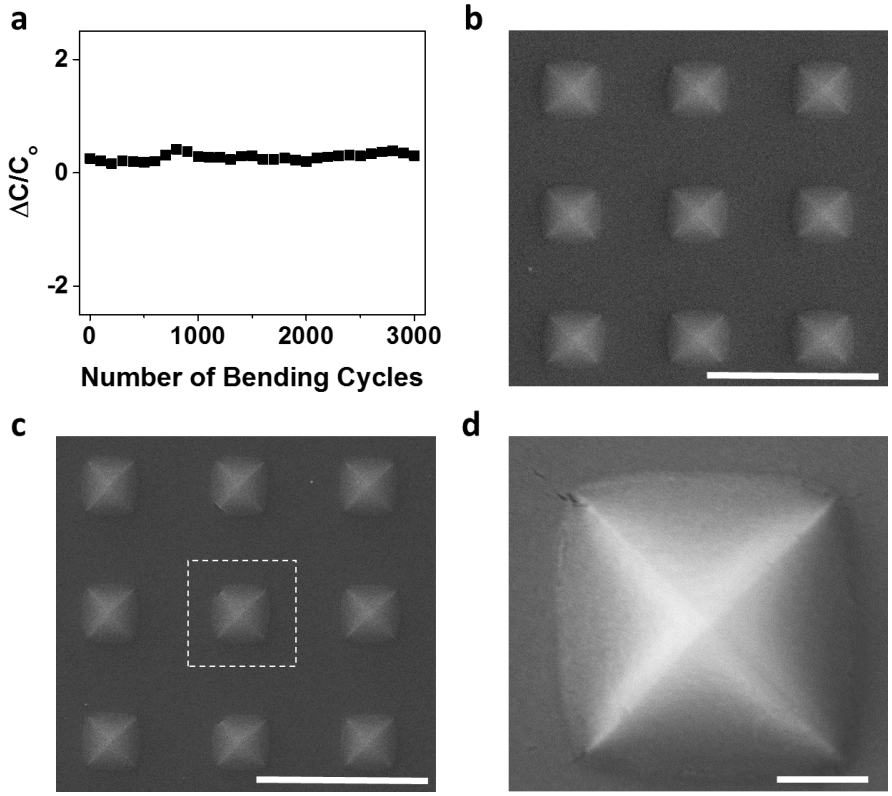

Figure 3-6 | Performance of the bending stability. (a) Bending stability test of the flexible CMAG capacitor-based E-skin responding to a load of 430 Pa on a curve surface with the bending radius ~ 32.5 mm. SEM images of top-view conductive microstructured pyramids **(b)** before and **(c)** after bending test. **(d)** Magnified SEM image extracted from the dash squared box in **c**. The scale bars in **b** and **c** are denoted as 20 μm. The scale bar in **d** represents 2 μm.

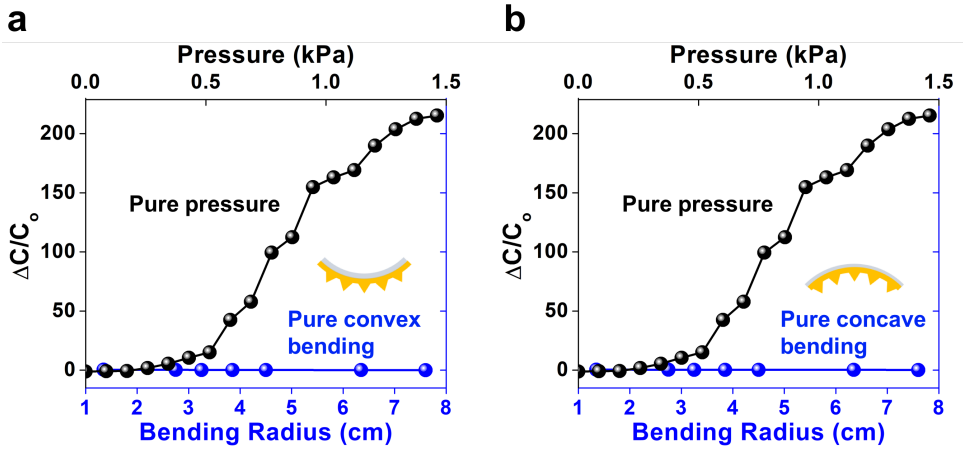

Figure 3-7 | Comparisons of flexing effect and pure pressure on the flexible CMAG capacitive E-skin. *ΔC/Co* corresponding to various pressure loads (top axis) *vs.* **(a)** pure convex bending and **(b)** pure concave bending with various radii, respectively (bottom axis).

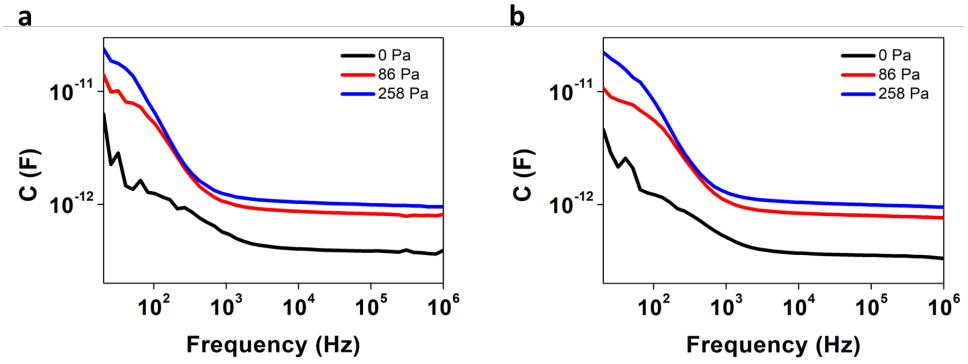

Figure 3-8 | Capacitance response of the flexible E-skin corresponding to the frequency range from 20 Hz to 10 MHz under the applied pressure of 0, 86, and 258 Pa. Capacitance *vs.* frequency measured at **(a)** 0.1 V_{rms} and **(b)** 1.5 V_{rms}.

References

1 Mannsfeld, S. C. *et al.* Highly sensitive flexible pressure sensors with microstructured rubber dielectric layers. *Nature materials* **9**, 859 (2010).

2 Schwartz, G. *et al.* Flexible polymer transistors with high pressure sensitivity for application in electronic skin and health monitoring. *Nat. Commun.* **4**, 1859 (2013).

3 Lee, B.-Y., Kim, J., Kim, H., Kim, C. & Lee, S.-D. Low-cost flexible pressure sensor based on dielectric elastomer film with micro-pores. *Sens. Actuator A-Phys.* **240**, 103-109 (2016).

4 Lei, K. F., Lee, K.-F. & Lee, M.-Y. A flexible PDMS capacitive tactile sensor with adjustable measurement range for plantar pressure measurement. *Microsys. Technol.* **20**, 1351-1358 (2014).

5 Zhang, B. *et al.* Dual functional transparent film for proximity and pressure sensing. *Nano Res.* **7**, 1488-1496 (2014).

6 Metzger, C. *et al.* Flexible-foam-based capacitive sensor arrays for object detection at low cost. *Appl. Phys. Lett.* **92**, 013506 (2008).

7 Zang, Y. *et al.* Flexible suspended gate organic thin-film transistors for ultra-sensitive pressure detection. *Nature communications* **6**, 6269 (2015).

8 Lee, H.-K., Chang, S.-I. & Yoon, E. A flexible polymer tactile sensor: fabrication and modular expandability for large area deployment. *J. Microelectromech. Syst.* **15**, 1681-1686 (2006).

9 Lee, J. *et al.* Conductive Fiber-Based Ultrasensitive Textile Pressure Sensor for Wearable Electronics. *Adv. Mater.* **27**, 2433-2439 (2015).

10 Pang, C. *et al.* Highly Skin-Conformal Microhairy Sensor for Pulse Signal Amplification. *Adv. Mater.* **27**, 634-640 (2015).

11 Park, S. *et al.* Stretchable Energy-Harvesting Tactile Electronic Skin Capable of Differentiating Multiple Mechanical Stimuli Modes. *Adv. Mater.* **26**, 7324-7332 (2014).

12 Boutry, C. M. *et al.* A Sensitive and Biodegradable Pressure Sensor Array for Cardiovascular Monitoring. *Adv. Mater.* **27**, 6954-6961 (2015).

13 Tee, B. C. K. *et al.* Tunable flexible pressure sensors using microstructured elastomer geometries for intuitive electronics. *Adv. Funct. Mater.* **24**, 5427-5434 (2014).

14 Lipomi, D. J. *et al.* Skin-like pressure and strain sensors based on transparent elastic films of carbon nanotubes. *Nature Nanotech.* **6**, 788-792 (2011).

Chapter 4: E-skins from CMAG-2D semiconductor transistors

A. Introduction of transistor-based E-skins for pressure sensing

Among different E-skins for pressure sensing, the transistor-based E-skins are particularly attractive for several reasons, such as signal amplification by directly converting the capacitance signal to source-drain current, the capability of integrating tactile sensors by constructing active matrix arrays that enable faster scan rates and less cross-talk between each pixel, *etc*. Recently, various fabrication techniques of the transistor-based pressure sensors have been developed including different kinds of the semiconducting channel materials (*i.e.*, organic semiconductors, carbon nanotubes (CNTs), graphene, nanowires, *etc.*[1-4]), the electrodes (*i.e.*, CNTs, metals, and the elastomers embedded with the conductive fillets), and the pressure-sensitive gate or dielectrics (*i.e.*, PSR, microstructured dielectrics, resistive tactile sensing foils and so on[5-8]); among these, the semiconducting channel materials offer distinct characteristics of the transistors, such as mobility, current on/off ratio, transconductance, threshold voltages, operation voltages, *etc.*, which strongly affect the pressure sensing performance of the E-skins.

For example, by laminating the organic field effect transistors (OFETs) with a PSR layer or microstructured elastic dielectrics, the organic transistor-based E-skins with high flexibility and low cost have been realized; however, these devices typically exhibit relatively low electrical performance, insufficient environmental stability, and large operation voltage up to 200 V, which are difficult to implement for practical applications[5,6,9,10]. Although inorganic semiconductor materials (*i.e.*, Si, indium gallium zinc oxide (IGZO), *etc.*) show excellent electrical performance (*e.g.*., high carrier mobilities, higher on/off ratio, ambient stability, *etc*.), they are usually rigid and

hard to implement especially for flexible and light-weight E-skins. Recently, 2D layered semiconductor materials (*i.e.*, MoS_2, WSe_2, *etc.*) have attracted attention because of their excellent electrical performance, outstanding mechanical properties, superior air stability, ultrathin thickness, and accessibility for flexible plastic subtracts, which might be the alternate solutions for high performance of the ultrathin robust electronics and related applications such as the conformal tactile sensors, E-skins for humidity sensing, *etc*.[11,12]

Herein, we present a new design of E-skins by integrating 2D semiconductor transistors with our unique pressure sensitive CMAG gate, which can overcome the challenges in current transistor-based E-skins: (1) relatively low inherent electrical performance from the organic transistors (*e.g.*, low on/off ratio, relatively low transconductance, degradation in the ambient condition, large operation voltage, *etc*.), (2) lower pressure sensitivity and (3) slower response caused by the viscoelastic behavior of the rubber dielectrics. With ultrahigh pressure sensitivity, faster response, lower power consumption, and low minimum detectable pressure, long-term stability and robustness, our CMAG-2D semiconductor E-skins deliver an overall performance well above the existing pressure-sensing E-skins, which would make a valuable contribution to the community of E-skins and related applications.

B. Pressure sensing performance of the CMAG-2D semiconductor E-skins

Here, we present a new design of E-skin integrating 2D semiconductor transistors with the CMAG gates (Fig. 2-2c). In our design, the CMAGs offer the "true" microstructured air gaps without unwanted effects caused by less compressible thick dielectric, and few-layer 2D materials

(*e.g.*, MoS_2 and WSe_2) are chosen as the semiconducting channel for their high mobility and high on/off ratio, excellent mechanical flexibility, and air stability[13-19]. Together, our design can lead to greatly improved sensitivity, along with ultrafast response, lower power consumption, and long-term stability and robustness. The pressure sensing performance of our devices can be determined by

$$I_{sd} = \frac{W}{L} \cdot \mu \cdot C_i \cdot (V_g - V_t) \cdot V_{sd} \qquad (4\text{-}1)$$

, where I_{sd}, V_{sd}, V_t, and V_g are the source-drain current and voltage, threshold voltage, and gate voltage, respectively; W, L, μ, and C_i are denoted as the channel width and length, mobility, and specific gate capacitance, correspondingly. It is obvious that the source-drain current is proportional to the specific gate capacitance that allows I_{sd} to respond quickly to the change in the applied pressure. By using the unique CMAGs as the gate for 2D semiconductor transistors, the applied pressure can readily vary the air-gap thickness within the CMAGs and the gate capacitance, which can be sensitively read out by the source-drain current.

The sensitivity and SNR of our devices are related to highly sensitive pressure-dependent CMAGs and the inherent electric performance of the transistors, such as transconductance, current on/off ratio, and threshold voltage. To achieve higher sensitivity and SNR of the devices, we operated our CMAG-MoS_2 E-skin near the regime with the highest transconductance, where the source-drain current can sensitively change upon a small pressure load, leading to an ultrahigh sensitivity. The CMAG-MoS_2 E-skin exhibits I_{sd} of ~ 1.45×10^{-6} A without applied pressure (Fig. 4-1a). As the applied pressure increases to 1.63 kPa, I_{sd} decreases dramatically by more than six orders of magnitude to off-state regime. The normalized channel resistance change ($\Delta R/R_o$, where

$\Delta R = R - R_o$; R and R_o are the channel resistance with and without pressure load, respectively) can reach more than ~ 4.63×10^6 (Fig. 4-1b). The pressure sensitivity of the E-skin, defined as $S = \delta(\Delta R/R_o)/\delta P$, can reach an unprecedented value up to ~ 2.61×10^7 kPa^{-1} (average sensitivity ~ 3.64×10^6 kPa^{-1}) in the pressure range of ~ 0−1.63 kPa (Fig. 4-1c). To the best of our knowledge, both the sensitivity and SNR represent the highest ever reported among all types of E-skins for pressure detection (~ 5.8×10^6, ~ 1.36×10^5, ~ 4 times greater than the sensitivity of current records of capacitor-, transistor-, and resistor-based pressure sensors, respectively)[3,5-10,20-39].

The CMAG-2D semiconductor transistor-based sensors can also be readily applied on flexible substrate. For example, we have fabricated CMAG-WSe_2 transistors on flexible polyimide (PI) substrate. The transfer curves of the flexible CMAG-WSe_2 E-skin exhibits the bipolar characteristics. Without the applied pressure, I_{sd} is ~ 4×10^{-11} A, indicating the off state. As the pressure increases, I_{sd} is enhanced strongly at negative V_g (Fig. 4-1d). The normalized source-drain current change ($\Delta I/I_o$, where $\Delta I = I - I_o$; I and I_o are the source-drain current with and without pressure load, respectively) can reach ~ 2×10^4 (Fig. 4-1e); the transfer curves of the flexible CMAG-WSe_2 E-skin also show a high pressure sensitivity up to 1.76×10^4 kPa^{-1} within the pressure range below 2.4 kPa (Fig. 4-1f).

C. Tunability of the pressure sensing performance

The sensing behaviors of the CMAG-2D semiconductor E-skins can be tailored by tuning the doping concentration of the semiconductor channel and selecting specific regions of the transfer curves from the transistors (*e.g.,* rapid switching and highest sensitivity when the device

is operated in the subthreshold region, or linear response in the linear region), which can be valuable for meeting the specific application requirements. The dielectrics on 2D semiconductor transistors may also be tailored to further lower the operation voltage and broaden the pressure sensing range while maintaining the high sensitivity and SNR. For example, with the optimized doping concentration of semiconductor material and dielectric, the CMAG-2D MoS_2 E-skin exhibits higher $\Delta R/R_o$ and sensitivity within the relatively wide pressure range of ~ 0−3.2 kPa compared to other ultrahigh sensitive pressure sensors[39] (typically pressure range < 1.5 kPa), along with lower power consumption from 9 pW to 270 nW (operation voltages, V_{sd} = 1 V and V_g ~ -3V) (Fig. 4-2), which is considerably lower than that of organic transistor-based pressure sensors (up to 200 V)[5,6].

D. Air stability and mechanical behaviors of the devices

Air stability and mechanical stability are important for electronic devices. As a result, we investigated the ambient stability of the 2D semiconductor transistors. For example, the MoS_2 transistor still maintain ~ 70 % of I_{sd} after 7 months at V_g = 60 V and V_{sd} = 1 V (Fig. 4-3). Notably, our current device is not packaged and may be further improved with proper packaging/encapsulation in future studies. Moreover, the stability test of our device responding to a load of 86 Pa shows that our E-skin maintains highly stable performance over 6,000 loading cycles (Fig. 4-4).

E. Summary

In summary, we have integrated the highly pressure-sensitive CMAG gate with 2D semiconductor transistors, demonstrating that the concepts of the CMAGs can be applied with different kinds of semiconductor materials (*e.g.*, MoS_2 and WSe_2) and different substrates (*e.g.*, flexible and rigid). The CMAG-2D semiconductor E-skins exhibit record-high pressure sensitivity ~ 2.61×10^7 kPa^{-1} (*vs.* 192 kPa^{-1} of the transistor-based pressure sensor reported previously[10]), ultrafast response < 0.1 ms (*vs.* 10 ms reported previously[6,10]), lower power consumption (~ 9 pW−270 nW), and low minimum detectable pressure ~ 0.05 Pa (*vs.* ~ 0.5 Pa in normal conversation environment reported previously[10]), outstanding stability and favorite pressure sensing tunability by controlling the doping concentration of the semiconductor channel, selecting specific regions of the transfer curves from the transistors, and optimizing the dielectrics.

F. Methods

Device fabrication. The flexible polyimide (PI) substrate was pre-treated by spin-coating few layers of PI as the smooth layers, followed by 30nm-thick Al_2O_3 deposition through ALD. For the fabrication of CMAG-MoS_2 E-skin and the flexible CMAG-WSe_2 E-skin, few-layer MoS_2 and WSe_2 were exfoliated from the commercially available crystals of molybdenite and tungsten diselenide onto SiO_2 substrate and pre-treated flexible PI substrate,respectively. Then, lithography process defines the source-drain electrodes, followed by metal deposition (Ti/Au: 20 nm/80 nm). A polymeric dielectric layer was fabricated by spin coating a dielectric solution (poly-4-vinylphenol (PVP) mixed with 4,4'-(Hexafluoroisopropylidene)diphthalic anhydride (HDA) and

triethylamine (TEA) in propylene glycol monomethyl ether acetate (PGMEA), followed by curing at 150 ^{o}C in air for 30−60 min[40], followed by an additional 5- or 10-nm-thick Al_2O_3 deposition by ALD. The CMAGs was then laminated on top of gate-absent MoS_2 and WSe_2 transistors to obtain CMAG- MoS_2 and flexible CMAG-WSe_2 transistor-based E-skin devices.

Device characterization. Electrical characterization of the CMAG-MoS_2 and CMAG-WSe_2 E-skin were done under ambient conditions using the Agilent B2902A or built-in data acquisition (DAQ) computer connected with low noise current preamplifier (SR570), and loads were applied by various weights. The cyclic loading test of the CMAG-2D semiconductor E-skin was done with pressure of 86 Pa on the flat surface.

G. Figures

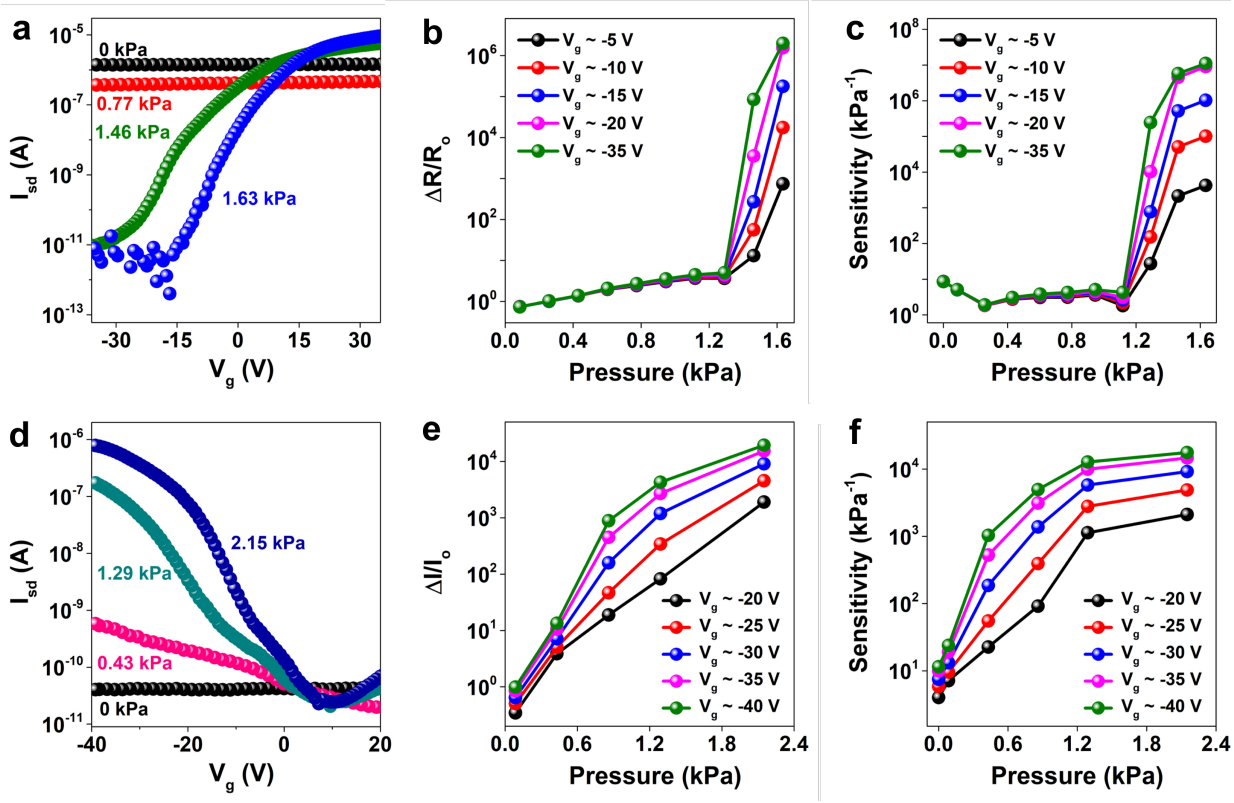

Figure 4-1 | Pressure sensing performance of the CMAG-2D semiconductor E-skin. (a) Transfer curves of the CMAG-MoS_2 E-skin on SiO_2 substrate at V_{sd} = 1 V under different pressure. **(b)** The normalized channel resistance change and **(c)** the corresponding sensitivity at V_{sd} = 1 V and different V_g. **(d)** Transfer curves of the flexible CMAG-WSe_2 E-skin on pre-treated PI substrate at V_{sd} = 1 V under various applied pressure. **(e)** The normalized source-drain current change and **(f)** the corresponding sensitivity at V_{sd} = 1 V and different V_g.

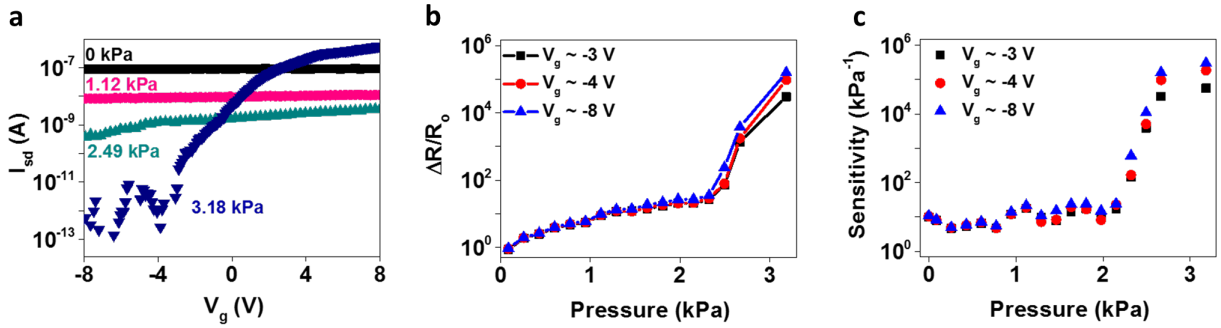

Figure 4-2 | Pressure sensing performance of the CMAG-MoS_2 E-skin with the optimized bottom dielectric. (a) Transfer curves of the CMAG-MoS_2 E-skin on SiO_2 substrate at lower threshold voltage (V_{sd} = 1 V) under various applied pressure. **(b)** The normalized channel resistance changes and **(c)** the corresponding sensitivity at constant V_{sd} = 1 V.

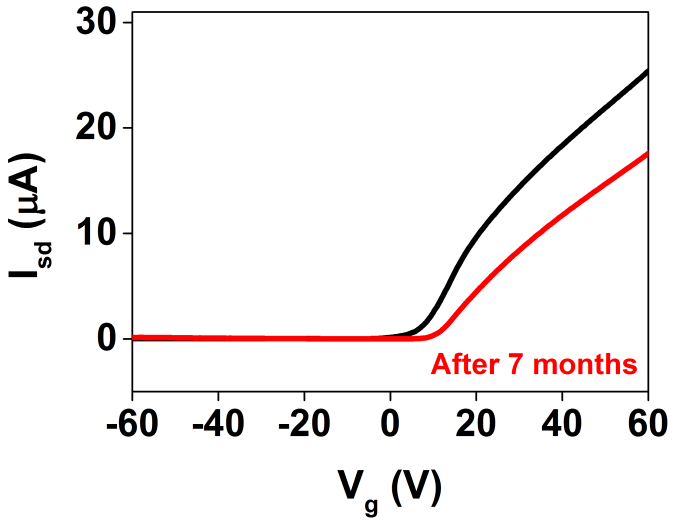

Figure 4-3 | Transfer curves of MoS_2 transistor before and after 7 months at V_{sd} = 1 V.

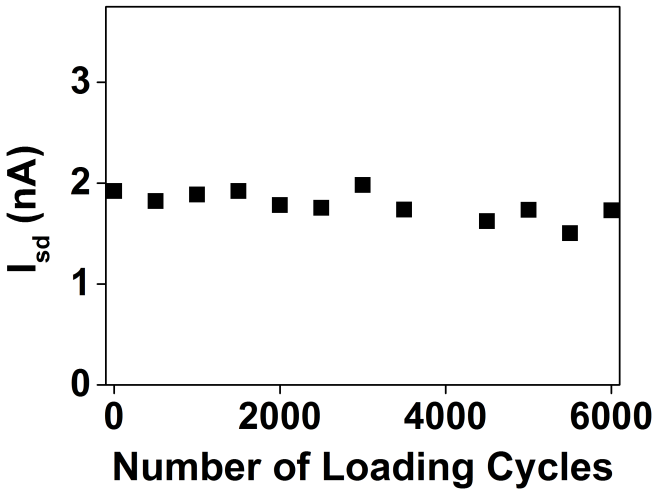

Figure 4-4 | Stability test of the CMAG-MoS_2 E-skin responding to a load of 86 Pa over 6,000 loading-unloading cycles at V_{sd} = 1 V.

References

1 Ji, T., Jung, S. & Varadan, V. K. Field-controllable flexible strain sensors using pentacene semiconductors. *IEEE Electron Device Letters* **28**, 1105-1107 (2007).

2 Cernetic, N. *et al.* Systematic Doping Control of CVD Graphene Transistors with Functionalized Aromatic Self-Assembled Monolayers. *Advanced functional materials* **24**, 3464-3470 (2014).

3 Takei, K. *et al.* Nanowire active-matrix circuitry for low-voltage macroscale artificial skin. *Nature materials* **9**, 821 (2010).

4 Chae, S. H. *et al.* Transferred wrinkled Al 2 O 3 for highly stretchable and transparent graphene–carbon nanotube transistors. *Nature materials* **12**, 403 (2013).

5 Mannsfeld, S. C. *et al.* Highly sensitive flexible pressure sensors with microstructured rubber dielectric layers. *Nature materials* **9**, 859 (2010).

6 Schwartz, G. *et al.* Flexible polymer transistors with high pressure sensitivity for application in electronic skin and health monitoring. *Nat. Commun.* **4**, 1859 (2013).

7 Someya, T. *et al.* Conformable, flexible, large-area networks of pressure and thermal sensors with organic transistor active matrixes. *Proceedings of the National Academy of Sciences of the United States of America* **102**, 12321-12325 (2005).

8 Kaltenbrunner, M. *et al.* An ultra-lightweight design for imperceptible plastic electronics. *Nature* **499**, 458 (2013).

9 Manunza, I. & Bonfiglio, A. Pressure sensing using a completely flexible organic transistor. *Biosens. Bioelectron.* **22**, 2775-2779 (2007).

10 Zang, Y. *et al.* Flexible suspended gate organic thin-film transistors for ultra-sensitive pressure detection. *Nature communications* **6**, 6269 (2015).

11 Park, M. *et al.* MoS2-based tactile sensor for electronic skin applications. *Advanced Materials* **28**, 2556-2562 (2016).

12 Guo, H. *et al.* Transparent, flexible, and stretchable WS 2 based humidity sensors for electronic skin. *Nanoscale* **9**, 6246-6253 (2017).

13 Chuang, H.-J. *et al.* High mobility WSe2 p-and n-type field-effect transistors contacted by highly doped graphene for low-resistance contacts. *Nano Lett.* **14**, 3594-3601 (2014).

14 Zhao, W. *et al.* Evolution of electronic structure in atomically thin sheets of WS2 and WSe2. *ACS nano* **7**, 791-797 (2012).

15 Bertolazzi, S., Brivio, J. & Kis, A. Stretching and breaking of ultrathin MoS2. *ACS nano* **5**, 9703-9709 (2011).

16 Radisavljevic, B., Radenovic, A., Brivio, J., Giacometti, V. & Kis, A. Single-layer MoS2 transistors. *Nature Nanotech.* **6**, 147-150 (2011).

17 Kim, S. *et al.* High-mobility and low-power thin-film transistors based on multilayer MoS2 crystals. *Nat. Commun.* **3**, 1011 (2012).

18 Zhao, M. *et al.* Large-scale chemical assembly of atomically thin transistors and circuits. *Nature Nanotechnology* (2016).

19 Cheng, R. *et al.* Few-layer molybdenum disulfide transistors and circuits for high-speed flexible electronics. *Nat. Commun* **5**, 5143 (2014).

20 Lipomi, D. J. *et al.* Skin-like pressure and strain sensors based on transparent elastic films of carbon nanotubes. *Nature Nanotech.* **6**, 788-792 (2011).

21 Pang, C. *et al.* A flexible and highly sensitive strain-gauge sensor using reversible interlocking of nanofibres. *Nature materials* **11**, 795 (2012).

22 Yeom, C. *et al.* Large-Area Compliant Tactile Sensors Using Printed Carbon Nanotube Active-Matrix Backplanes. *Adv. Mater.* **27**, 1561-1566 (2015).

23 Sekitani, T. *et al.* Organic nonvolatile memory transistors for flexible sensor arrays. *Science* **326**, 1516-1519 (2009).

24 Someya, T. *et al.* A large-area, flexible pressure sensor matrix with organic field-effect transistors for artificial skin applications. *Proc. Natl. Acad. Sci. USA* **101**, 9966-9970 (2004).

25 Park, S. *et al.* Stretchable Energy-Harvesting Tactile Electronic Skin Capable of Differentiating Multiple Mechanical Stimuli Modes. *Adv. Mater.* **26**, 7324-7332 (2014).

26 Boutry, C. M. *et al.* A Sensitive and Biodegradable Pressure Sensor Array for Cardiovascular Monitoring. *Adv. Mater.* **27**, 6954-6961 (2015).

27 Pang, C. *et al.* Highly Skin-Conformal Microhairy Sensor for Pulse Signal Amplification. *Adv. Mater.* **27**, 634-640 (2015).

28 Lee, J. *et al.* Conductive Fiber-Based Ultrasensitive Textile Pressure Sensor for Wearable Electronics. *Adv. Mater.* **27**, 2433-2439 (2015).

29 Zhang, B. *et al.* Dual functional transparent film for proximity and pressure sensing. *Nano Res.* **7**, 1488-1496 (2014).

30 Tee, B. C. K. *et al.* Tunable flexible pressure sensors using microstructured elastomer geometries for intuitive electronics. *Adv. Funct. Mater.* **24**, 5427-5434 (2014).

31 Lee, H.-K., Chang, S.-I. & Yoon, E. A flexible polymer tactile sensor: fabrication and modular expandability for large area deployment. *J. Microelectromech. Syst.* **15**, 1681-1686 (2006).

32 Metzger, C. *et al.* Flexible-foam-based capacitive sensor arrays for object detection at low cost. *Appl. Phys. Lett.* **92**, 013506 (2008).

33 Lei, K. F., Lee, K.-F. & Lee, M.-Y. A flexible PDMS capacitive tactile sensor with adjustable measurement range for plantar pressure measurement. *Microsys. Technol.* **20**, 1351-1358 (2014).

34 Pan, L. *et al.* An ultra-sensitive resistive pressure sensor based on hollow-sphere microstructure induced elasticity in conducting polymer film. *Nature communications* **5**, 3002 (2014).

35 Noguchi, Y., Sekitani, T. & Someya, T. Organic-transistor-based flexible pressure sensors using ink-jet-printed electrodes and gate dielectric layers. *Appl. Phys. Lett.* **89**, 3507 (2006).

36 Takahashi, T., Takei, K., Gillies, A. G., Fearing, R. S. & Javey, A. Carbon nanotube active-matrix backplanes for conformal electronics and sensors. *Nano Lett.* **11**, 5408-5413 (2011).

37 Graz, I. *et al.* Flexible active-matrix cells with selectively poled bifunctional polymer-ceramic nanocomposite for pressure and temperature sensing skin. *J. Appl. Phys.* **106**, 034503 (2009).

38 Lai, Y. C. *et al.* Extraordinarily Sensitive and Low-Voltage Operational Cloth-Based Electronic Skin for Wearable Sensing and Multifunctional Integration Uses: A Tactile-Induced Insulating-to-Conducting Transition. *Adv. Funct. Mater.* **26**, 1286-1295 (2016).

39 Lee, S. *et al.* A transparent bending-insensitive pressure sensor. *Nat Nanotechnol* **11**, 472-478 (2016).

40 Roberts, M. E. *et al.* Cross-linked polymer gate dielectric films for low-voltage organic transistors. *Chem. Mater.* **21**, 2292-2299 (2009).

Chapter 5: Applications of CMAG E-skins

A. Introduction of various applications in E-skins

E-skin is an artificial skin with human-like sensory capabilities, which can sense pressure, temperature, pain, and other external stimuli. In order to mimic human skin, different kinds of sensors or electronic devices (*i.e.*, pressure sensors, temperature sensors, magnetic sensor, *etc*.) are embedded within the soft substrates (*i.e.*, PI, PET, PDMS, Ecoflex materials, *etc*.). Recently, various E-skins and related applications have been widely developed due to the increasing demand for flexible electronic devices such as wearable healthcare monitoring, human-machine interface (HMI), robotic technologies, *etc.* (Fig. 5-1)[1-21]; among these, the pressure-sensitive E-skins with the capability that transduces an applied force into an electrical signal have attracted significant attention due to their important applications in health monitoring, robotic technologies, microelectromechanical systems (MEMS), microphones, hearing aids and so on[2,5,19,22-29]. However, the applications of current pressure-sensitive E-skins are still limited by their relatively low sensing performance (*e.g.*, low pressure sensitivity, slower response, large operation voltage, degradation in the ambient condition and so on) due to the technical challenges of device architecture design and fabrication processes.

With the unique design of the CMAGs, our capacitor- and transistor-based E-skins for pressure sensing exhibit unprecedented pressure sensing performance. In this chapter, we show that the CMAG capacitor-based E-skins can be used as wearable health monitoring devices to detect the human pulse waves and obtain the related health information. Moreover, the highly sensitive static pressure mapping suggests that our CMAG capacitive E-skin arrays have the ability

for detecting the pressure locations and the corresponding pressure levels, which might be used for future touch devices.

By integrating the pressure sensitive CMAG gate with 2D semiconductor transistors, our CMAG-2D semiconductor E-skins show ultrahigh pressure sensitivity, faster response, low power consumption, long-term stability and robustness, which can be used as "E-skin microphone" for acoustic wave detection and speech pattern recognition. Moreover, by integrating the CMAG E-skins with a system on chip (SoC) and related circuits, the remote pressure monitoring can be realized allowing users to obtain the pressure sensing information from their mobile devices directly.

B. Highly sensitive pressure mapping for touch devices

In order to meet the application requirements for healthcare and HMI, it is essential to scale up E-skin devices and to create sensory arrays for monitoring the spatial distribution of the pressure information. As a demonstration, we fabricated a flexible 5 × 5 pixel array of the CMAG capacitance-based E-skin with the total device area ~ 2.5 × 2.5 cm^2 and the area of each pixel ~ 6 mm^2 (Fig. 5-2 a-b). The E-skin array was fabricated by orthogonally integrating 5 stripe-patterned CMAGs as top electrodes (~ 2.5-mm wide) with 5 parallel electrodes (~ 2.5-mm wide Au strip with the 30 nm-thick Al_2O_3 dielectric) on PET substrate. For pressure mapping test, grains of rice, soybean, and red bean (with the weight ~ 20, 158, and 219 mg, respectively) were placed on different pixels in the arrays, and the corresponding normalized capacitance change distribution of E-skin clearly shows the response of our device to the placement of different grains, where the

brighter color pixel indicates a higher capacitance sensed (Fig. 5-2a). Three brighter spots corresponding to the greater compression suggest the locations of the grains and the corresponding pressure variation. Notably, the pressure of a rice grain ~ 12.25 Pa requires a highly sensitive pressure sensory array to distinct the applied pressure level and location, that is beyond the typical pressure sensing range of the E-skins reported previously (~ 1 kPa−1 MPa pressure range[19,24,26,30]). We also placed a penny (with the weight of 3.11 g) on the E-skin arrays, and the normalized capacitance change clearly maps the pressure distribution corresponding to the location of a penny (Fig 5-2b).

C. Wearable CMAG E-skins for human pulse wave monitoring

The wearable healthcare devices are of considerable interest for telemedicine and prevention of the cardiovascular diseases (CVDs). For example, CVDs (*i.e.*, atherosclerosis, stroke, arrhythmia, *etc.*) are the leading causes of disability and death globally[31]. The wearable E-skin as a smart device provides a comfortable and non-invasive way to continually monitor the pulse wave of the radial artery for early detection and prevention of CVDs. Moreover, by using thinner PET substrate, the tattoo-like CMAG E-skin can provide more comfortable wearing experience (Fig. 5-3a-b). Our CMAG E-skin shows the ability to monitor the real-time human pulse waves while we attached it on the position above the radial artery of an adult human wrist. Subject A is 169-cm-tall female and B is 186-cm-tall male; both are in their late 20s to early 30s. At rest, the pulse wave signals of two subjects A and B show the heart rates of 82 b.p.m. and 77 b.p.m, respectively (Fig. 5-3d); both are within the normal range between 60−100 b.p.m. After 3-minute exercising, both heart rates of subjects A and B increase to 135 b.p.m. and 157 b.p.m.,

accordingly. (Fig. 5-3d). Different subjects show clearly distinct heartbeat patterns but similar trend (their heart-rates increase after exercise), indicating that our device is very reliable and stable for distinct human subjects; noticeably, the clear breath patterns from the sensing signals can be seen in four different subjects (Fig. 5-3d, Fig. 5-4). At rest, the characteristic pulse wave exhibits two clearly distinguishable peaks−percussion peak (P_1) and diastolic peak (P_3), along with a late augmentation shoulder (P_2) (Fig. 5-3e). The shape of pulse wave is caused by the contraction of the left ventricle and a reflected wave from the lower body, enabling to diagnose the arterial stiffness from the common used parameters such as Reflection Index (*R.I.*) = (P_2/P_1) × 100 % and Arterial Stiffness Index (*S.I.*) = human subject height (in unit of meter)/transit time (ΔT_{DVP}, in unit of second). The transit time is defined as the time delay between first and second peaks[32,33]. At rest, *R.I.* and *S.I.* were calculated to be 61.3 % and 6.67, respectively, indicating a healthy state of an adult female. After 5-minute exercise, the late systolic augmentation (P_2) disappears (Fig. 5-3e), which can be attributed to several reasons such as large artery stiffness/PWV, altered heart rate/ventricular ejection characteristics and so on[34]. Notably, the real-time pulse wave signals can be obtained at very low operation voltage of 0.1 V_{rms} (Fig. 5-5), suggesting that our CMAG device is very sensitive even in the smaller voltage level. In the future, we may integrate the E-skin on the back of watch band to realize the smart device for monitoring the important indices related to CVDs (Fig. 5-3c).

D. CMAG E-skin microphone for acoustic wave detection and speech pattern recognition

Our CMAG E-skin is designed for the lower pressure range, especially in sound pressure range. To evaluate the response and sensitivity performance of our device in detecting the subtle

and extremely fast vibration caused by the acoustic waves, we placed CMAG device near a computer-controlled speaker. The sound pressure level from the speaker was measured by a sound meter (background noise in our lab is at ~ 62 dB). We applied higher frequency sound wave for evaluating the response time instead of using z-motor to apply pressure, in order to probe rapid response time of our device, which far exceeds the movement frequency of typical z-motors. With our CMAG design, a signal is only observed when the sound wave is transferred to the bottom side of the CMAGs. The response time is therefore defined as the time response of the current change when the compression is applied (increase of the capacitance and change of current, at the point the compressive mechanical wave traveled to the bottom side of the CMAGs) and removed (decrease of capacitance and reverse change of current at the point the releasing mechanical wave traveled to the bottom side of the CMAGs). Therefore, when an 8 kHz acoustic wave was applied and detected by our device (80.2 dB, the corresponding pressure ~ 0.2 Pa), a maximum response speed is ~ 0.03125 ms (considering one period ~ 0.125 ms, including 2 increases and 2 decreases in applied pressure, resulting in a response time ~ 0.125/4 ms), which is actually the limit of our measurement setup instead of the intrinsic limit of the device (Fig. 5-6a, Supplementary Movie 1-2). Furthermore, we show our E-skin can respond the acoustic waves at 4 kHz and 8 kHz with clear peaks and valleys matching with the expected acoustic wave frequency (Fig. 5-6a-b), indicating sufficient time response to such high frequency sound wave. Although mechanical waves (*i.e.*, sound pressure) traveling from the top to the bottom between our CMAGs (PET/microstructured-PDMS/Au) and the conventional (PET/Au/microstructured-PDMS) take roughly the same amount of time (Fig. 2-3a), the speed of a given detector is highly dependent on the "effective gain" between "mechanical" input and "electrical" output (*i.e.*, effective amplification of the sensing signals above the noise level). The ultrahigh pressure sensitive gate

capacitance and high transconductance of our E-skin greatly amplifies the source-drain current signal in response to the small change of the sound pressure. As a result, under the same acoustic wave, the sensing signals of our CMAG devices can be effectively amplified and distinguished form the noise (in stark contrast to the lower sensitivity device from the conventional microstructures), leading to faster response.

With unique merit of our design, we showed that our device could work as an "E-skin microphone", which requires high sensitivity and fast response time for accurate conversion of the subtle sound pressure to the electrical signals. We recorded the source-drain current change while applying different sound pressure levels within the frequency range from 50 to 8,000 Hz. The pressure sensitivity was obtained by differentiating the normalized current with the applied pressure. Our pressure sensor responds to an acoustic wave at wide frequency range (Fig. 5-7a). It is interesting to note that the device exhibits higher sensitivity of up to 820 kPa^{-1} (average sensitivity ~ 119 kPa^{-1}) in broader frequency range. Additionally, we recorded the source-drain current change when we applied an acoustic wave at 500 Hz with various sound pressure levels, and show that the CMAG-MoS_2 E-skin exhibits the minimum pressure detection of 0.05 Pa (*vs.* typically < 0.5 Pa of others in the normal conversation environment[19]) with excellent *linear* response in logarithm scale and the corresponding sensitivity ~ 146 kPa^{-1} (Fig. 5-7b).

Furthermore, we explore our device as an "E-skin microphone" to detect the music sound and human speech, and even differentiate the gender of the speakers and convert the measured sound pressure to the real voice signal. The repeatable, real-time, source-drain current variations were recorded while music was played (at 94 dB, the corresponding pressure ~ 1 Pa), clearly demonstrating that our devices with high sensitivity and fast response are able to distinguish

different types of music sounds (Fig. 5-8a-c, Supplementary Movie 3). Moreover, our E-skin might be used as a speech pattern recognition system in human-robot communication, authentication system, aids of speech visualization in teaching/learning languages, wearable speech training aids for the deaf[35-37], *etc.* The comparisons of the acoustic waveform measured by a standard microphone and our device show highly similar characteristic peaks and valleys of different words and sentences such as "UCLA", "Electronic skin", and "The important thing is not to stop questioning" at ~ 85 dB (the corresponding pressure ~ 0.356 Pa) (Fig. 5-9a, Fig. 5-10a-b). In order to give us more visual representation of an acoustic signal, we converted the measured source-drain current corresponding to time to the auditory spectrograms by using the short-time Fourier transform (STFT) (Fig. 5-9b). The repeatable characteristic peaks and patterns of the acoustic waveforms and the auditory spectrograms suggest that our E-skin is very reliable and stable for recognizing the specific words and sentences. Furthermore, we have successfully converted the signals measured by our E-skin back to the voice signals (Supplementary Voice 1); To the best of our knowledge, no such demonstration has been achieved before partly limited by insufficient pressure sensitivity or response speed of the E-skins. Moreover, our "E-skin microphone" is also capable of speech classification between female and male speakers by transferring the sensing signals from the time domain to the frequency domain through Fourier transform, which clearly shows distinct frequency regime for the male voice (primarily in the low frequency range 0–1,000 Hz) and the female voice (in wide frequency range 0–2,000 Hz), independent off the exact words spoken. (Figure 5-11).

E. Remote pressure monitoring

Additionally, by integrating high sensitive CMAG E-skin with a system on chip (SoC) and related circuits serving as a platform of the signal transduction from externally applied stimuli to electrical signal, conditioning and processing, the pressure signals detected by our device can be transmitted to the user's cell phones or computers, which provides the real-time remote pressure monitoring (Fig. 5-12) allowing to share the pressure sensing information, such as speech patterns or health information (heartbeat pattern and related parameters for diagnosis of arterial stiffness) with remote doctors.

F. Summary

In summary, we have demonstrated that the CMAG capacitor-based sensory arrays can be used for highly sensitive static pressure mapping requiring the low minimum detectable pressure (*i.e.*, the pressure of a rice grain ~ 12.25 Pa), which is beyond the typical pressure sensing range of the E-skins reported previously (~ 1 kPa−1 MPa)[19,24,26,30]. In addition, the CMAG E-skin provides comfortable and non-invasive way to detect the human pulse waves, allowing to obtain the valuable health information (*e.g.*, heartrate and breath patterns, *R.I.*, *S.I.*, *etc.*) for early detection and prevention of CVDs. Notably, it is also possible to directly obtain the pulse wave signals without further signal processing, such as amplifying, filtering, and smoothing, that is also important and convenient for the practical wearable health monitoring.

Moreover, we explore our CMAG device as an "E-skin microphone" with higher sensitivity of up to 820 kPa^{-1} (average sensitivity ~ 119 kPa^{-1}) in broader frequency range and

faster response (< 0.1 ms *vs.* 10 ms reported previously[19,27]), which can be used as the sound wave detections and speech pattern recognition to differentiate the gender of the speakers and enables to convert the measured signals back to the voice signals. We noticed that such signal conversion from sound pressure to voice signals has not been achieved with other E-skins, partly limited by insufficient pressure sensitivity and response speed of E-skins reported previously. In addition, our sensor achieves the minimum detectable pressure < 0.05 Pa (the background noise of our lab environment is at ~ 62 dB, corresponding to the pressure ~ 0.025 Pa), which is considerably smaller than the current state of the art (typically < 0.5 Pa[19] in the normal conversation environment).

Finally, the integration of the CMAG E-skin with system on chip (SoC) enables real-time remote pressure monitoring allowing to share the pressure information, such as speech patterns or health information (heartbeat pattern and related parameters for diagnosis of arterial stiffness) with remote doctors. We believe that the concepts of CMAGs and related applications will pave a new way for next generation of electronics and their applications.

G. Methods

Highly sensitive static pressure mapping. A flexible 5 × 5 capacitance-based E-skin array was assembled by orthogonally laminating 5 conductive microstructured PDMS strips (~ 2.5 mm wide, supported on PET supporting layer) on 5 parallel electrodes strip (~ 2.5 mm wide, covered by 30-nm-thick Al_2O_3 dielectric) on PET substrate. The parallel electrodes were deposited by e-beam evaporation of Cr/Au (20 nm/80 nm), and Al_2O_3 dielectric was deposited by atomic layer deposition (ALD). The total area of array is 2.5 × 2.5 cm^2 and the area of each pixel is ~ 6 mm^2.

Capacitance measurements were taken using the Agilent E4980A LCR meter (at 1 MHz frequency, oscillator's voltage level at 1.5 V_{rms} without DC bias) under ambient conditions. Pressure was applied by placing grains of rice, red bean, soy bean, and one penny on the capacitive E-skin array.

Wearable CMAG E-skins for human pulse wave monitoring. The device for human pulse wave measurement assembled by laminating the top stack (CMAGs/125-μm-thick PET) on the bottom stack (30 nm Al_2O_3/80 nm Au/125-μm-thick PET) with the overlapping area ~ 1 × 1 cm^2; we could also use thinner PET (with thickness from 4.8 to 70 μm) covered by transparent Tegaderm to realize tattoo-like E-skin for comfortable wearing experience (Fig. 5-3 a-b). Human pulse wave measurement was carried out by attaching the flexible capacitance-based E-skin to the wrist, with the CMAG side facing the skin. The pulse wave signals of four subjects including 2 females and 2 males were measured by two independent devices with the same structure and materials (Subjects A and C shown in Fig. 5-4 were measured by one device in June, 2016; Subject A, B (Fig. 5-3), and D (Fig. 5-4) were measured by a different device in May, 2018. Subject A were recorded two times with 2-year differences.

CMAG E-skin microphone. The "E-skin microphone" was fabricated by laminating the CMAGs supported on the 125-μm-thick PET or PI substrate (with thickness from 70-125 μm) with MoS_2 transistors covered by ~ 30-nm-thick polymeric dielectric and 30-nm-thick Al_2O_3 on Si substrate. For the measurements of acoustic wave detection and speech pattern classification, a computer-controlled speaker was served as an acoustic source while continuously recording the I_{sd} at constant voltages (V_{sd} = 1 V) by using Agilent B2902A or built-in data acquisition (DAQ) computer connected with low noise current preamplifier (SR570) under ambient condition. A sound meter

was used to measure the sound pressure level produced by the speaker (in units of decibels, dB). As a result, the sound pressure (P) can be defined by the following equation:

$$P \text{ (in unit of } Pa) = P_o 10^{\left(\frac{L_{dB}}{20}\right)}$$

, where P_o = 20 μPa (the reference sound pressure in air) and L_{dB} denotes measured sound pressure level. Response time measurement was recorded the I_{sd} change corresponding to the applied sound pressure at different frequencies. Measurement of sound pressure sensitivity corresponding to different frequencies and response time of our devices were obtained by recording the I_{sd} at constant V_{sd} = 1 and V_g = 30 V corresponding to a specific acoustic wave at frequency from 50 to 8,000 Hz. By recording I_{sd} change at 500 Hz corresponding to different sound pressure levels, the minimum pressure detection measurement was obtained. Notably, with higher pressure sensitivity and faster response speed of our design, our "E-skin microphone" is able to detect rapid and subtle sound pressure variations allowing the faithful signal conversion without attaching on the human subjects; on the contrary, most other E-skin devices are usually attached on the position nearby human throat in order to detect the relatively large pressure variations due to the vibration of vocal cord. Therefore, our "E-skin microphone" can function more like the standard microphone (both are sensitive to the rapid subtle sound pressure vibration unlike most E-skins that detect relatively large physical contact pressure caused by the human muscle contraction). For the speaker gender classification, the measured signals, I_{sd}, recorded from our "E-skin microphone" was converted from time domain to frequency domain by Fourier transform. All the signal processing for "E-skin microphone" demonstrations was done by using MATLAB.

Remote pressure monitoring. The CMAG-MoS_2 E-skin was used for the demonstration of the remote pressure monitoring (please see the detail device fabrication processes in Section F. Methods, Chapter 4) For remote pressure sensing and reading, a Raspberry Pi microcomputer was integrated with the CMAG-MoS_2 E-skin for transmitting the signal to remote computer or cell phone. The variation of source-drain current at constant voltages was recorded by the system and the results can be accessed through the Internet, so the current response upon the pressure applied by the finger can be monitored remotely. All control and application programs were written in Python language.

H. Figures

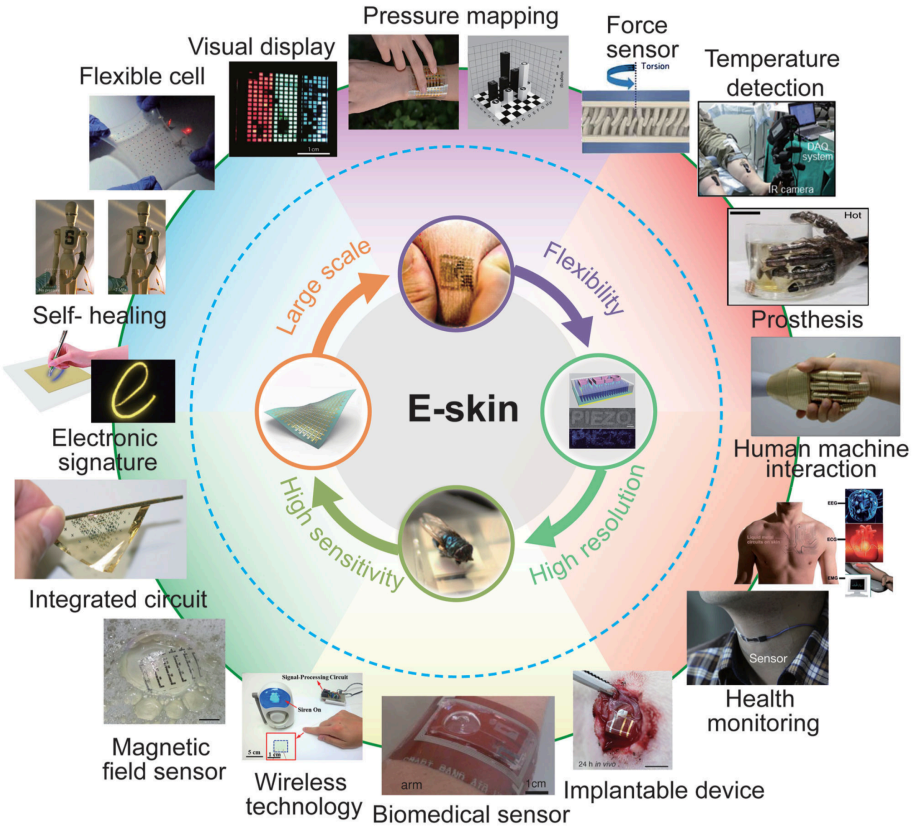

Figure 5-1 | Different kinds of E-skins and their applications. *Adapted from ref.* [1-21]

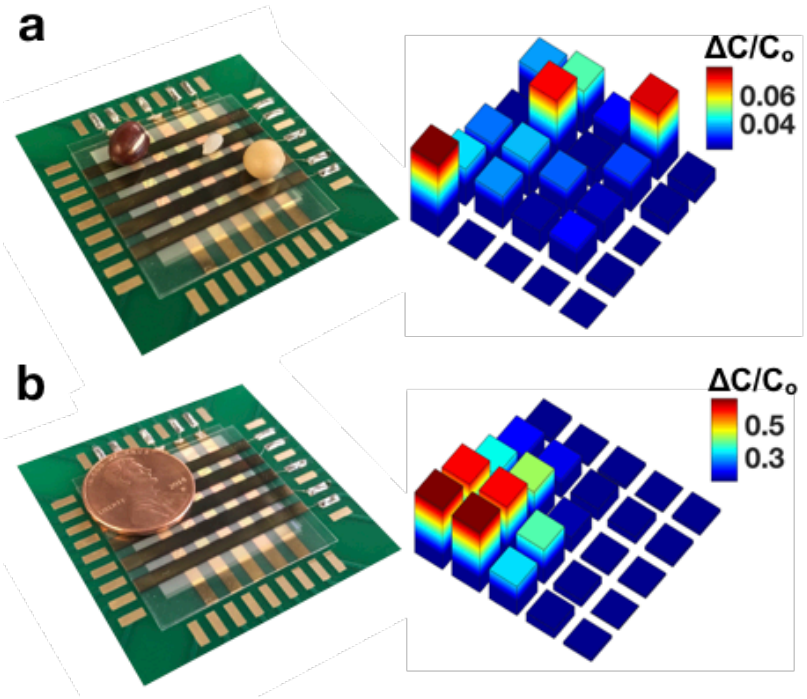

Figure 5-2 | Flexible CMAG capacitor-based E-skin for static pressure mapping. (a) Perspective view of a 5 × 5 pixel array upon placing grains of rice, soybean, and red bean with the weight ~ 20, 158, and 219 mg, respectively (left), and the corresponding distribution of the normalized capacitance change on the sensor array (right). **(b)** Perspective view of a 5 × 5 pixel array upon placing a penny with the weight 3.11 g (left), and the corresponding distribution of the normalized capacitance change (right).

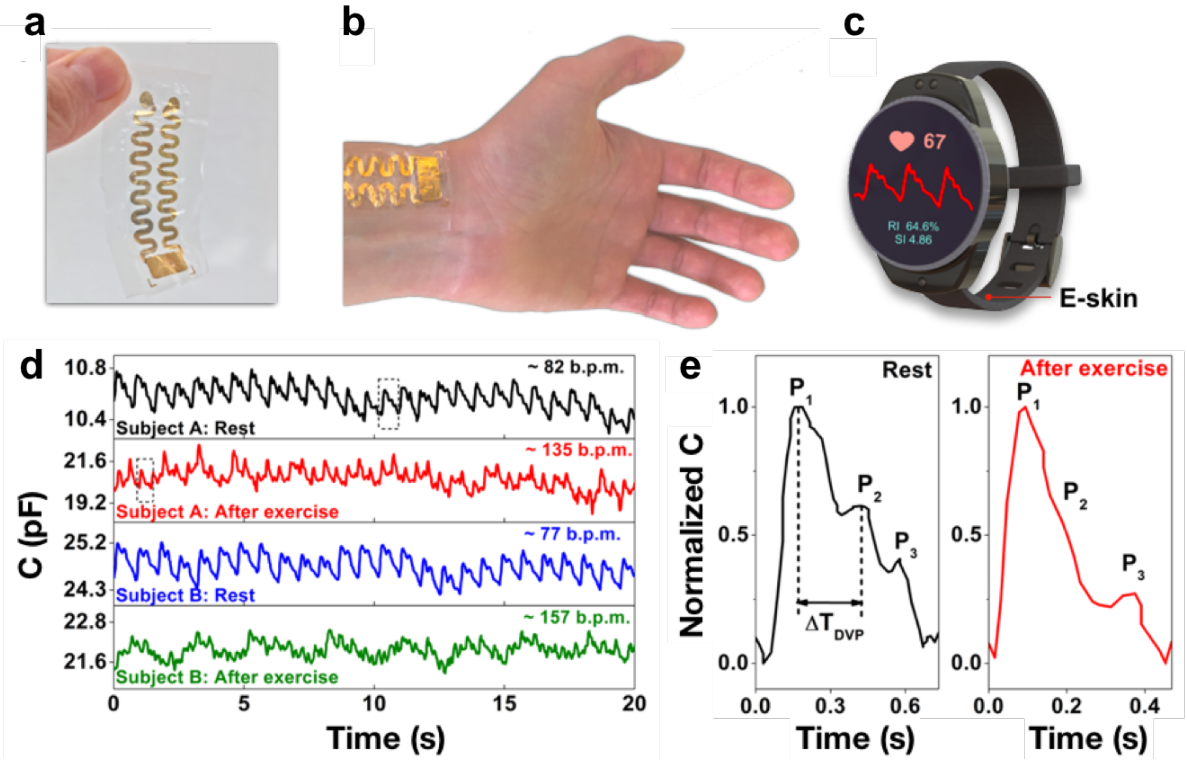

Figure 5-3 | Flexible CMAG capacitor-based E-skin for real-time pulse wave monitoring of the radial artery. (a) Image of flexible and comfortable tattoo-like E-skin. **(b)** Photograph of the E-skin attached on the position nearby the wrist artery. **(c)** Concept of the wearable smart device with the CMAG E-skin embedded on the back of device band for detecting health information (*i.e.*, heart rate, *R.I.*, and *S.I.*). **(d)** The real-time pulse wave monitoring of human subjects A and B before and after 5-minute exercise. **(e)** Comparisons of the zoomed-in waveforms of human subject A before and after 5-minute exercise extracted from the dashed square boxes in **d** showing the important health monitoring information such as Reflection Index (*R.I.*) = (P_2/P_1) × 100 % and Arterial Stiffness Index (*S.I.*) = subject height/ΔT_{DVP} (in unit of m/s).

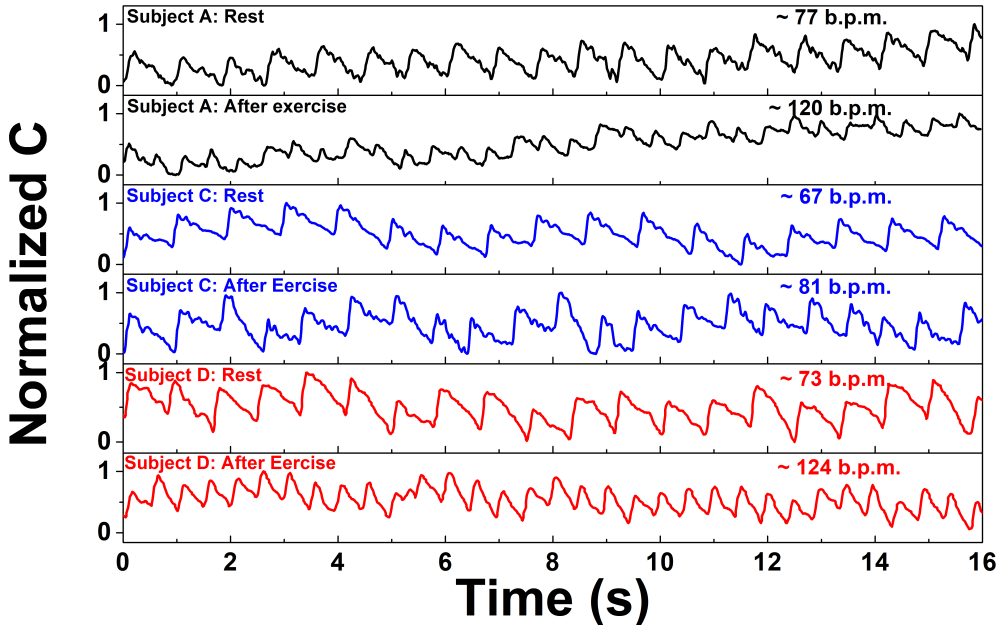

Figure 5-4 | Flexible CMAG capacitor-based E-skin for real-time pulse wave monitoring of the radial artery. The real-time pulse wave monitoring of human subjects A (169-cm-tall female), B (186-cm-tall male), C (181-cm-tall male), and D (161-cm-tall female) before and after 5-minute exercise. They are in their late 20s to early 30s. Subject A and C were measured by one device in June, 2016. Subject A, B and D were measure by a different device in May, 2018 (The data for subject A and B are shown in Figure 5-3d).

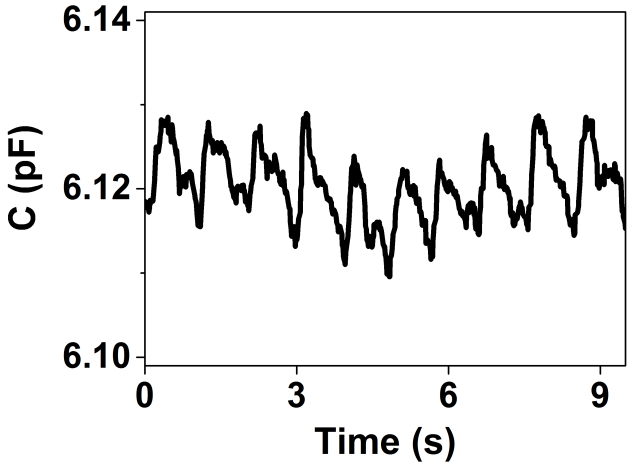

Figure 5-5 | The real-time wrist pulse wave monitoring over 9.5-second period at very low operation voltage, 0.1 V_{rms}. The pulse wave indicates the resting heart rate is ~ 63 b.p.m.

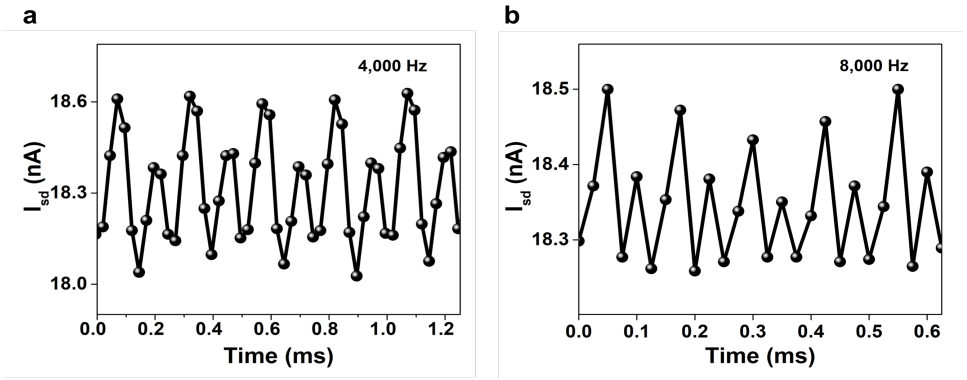

Figure 5-6 | The source-drain current response of CMAG-MoS_2 E-skin to a sound pressure at a fixed frequency of (a) 4 kHz and **(b)** 8 kHz, showing the consistent frequency response and highlighting the rapid response of our E-skin device to high frequency sound pressure signals.

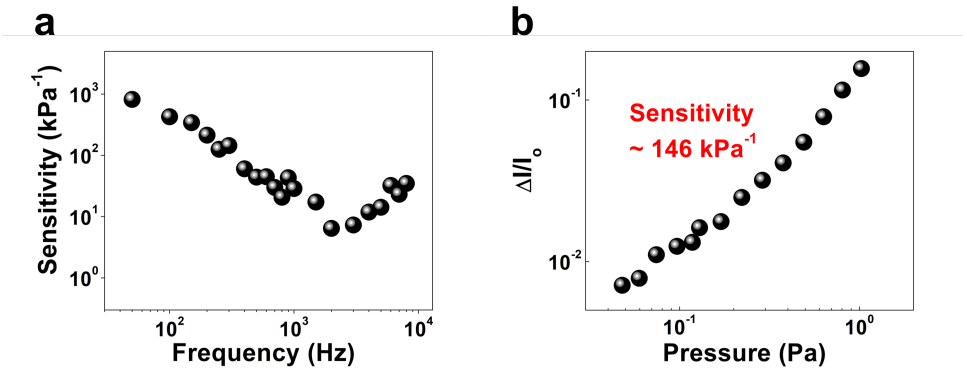

Figure 5-7 | The performance of E-skin microphone. (a) Sound pressure sensitivity corresponding to an acoustic wave at different frequencies. **(b)** Sound pressure response in the ultralow pressure range < 1 Pa with the excellent linearity of pressure sensitivity in logarithm scale.

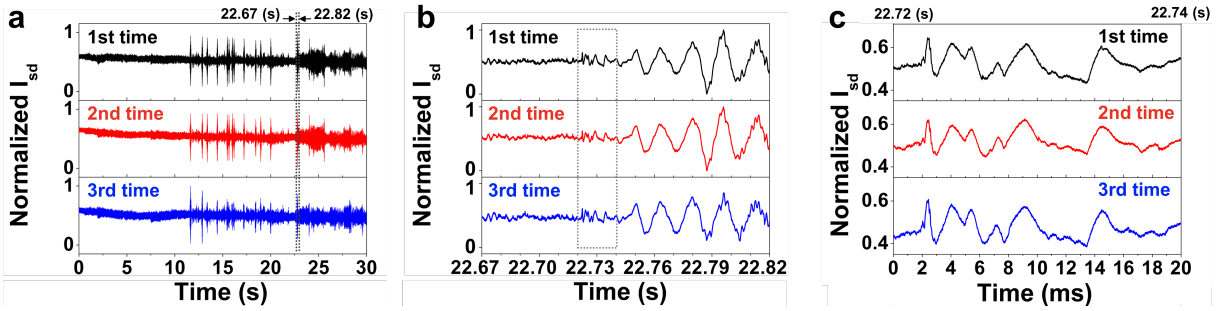

Figure 5-8 | The CMAG-MoS_2 E-skin for acoustic wave detection. (a) Electrical signal response of our device to the same music for three times at 94 dB. **(b)** Zoomed-in waveforms extracted from **a** showing the clearly distinct peaks and valleys. **(c)** Zoomed-in waveforms within the time duration from 22.72 to 22.74 s extracted from **b** showing high fidelity recognition of the music signal.

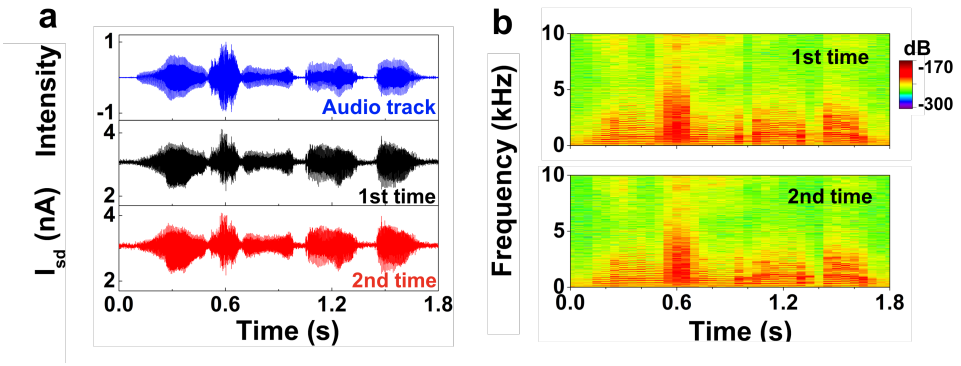

Figure 5-9 | The CMAG-MoS_2 E-skin for speech pattern recognition. (a) Comparisons of the acoustic waves measured by a standard microphone (top figure) and our E-skin (two figures at the bottom), respectively. The source-drain current response of our device was measured twice at constant V_{sd} = 1 V, while a speaker was played a non-native female speaker saying "U-C-L-A" at 85 dB. All the measurements were carried out in the normal conversation environment (~ 62 dB). **(b)** Auditory spectrograms of our device corresponding to two bottom figures in **a**, highlighting high fidelity speech pattern recognition.

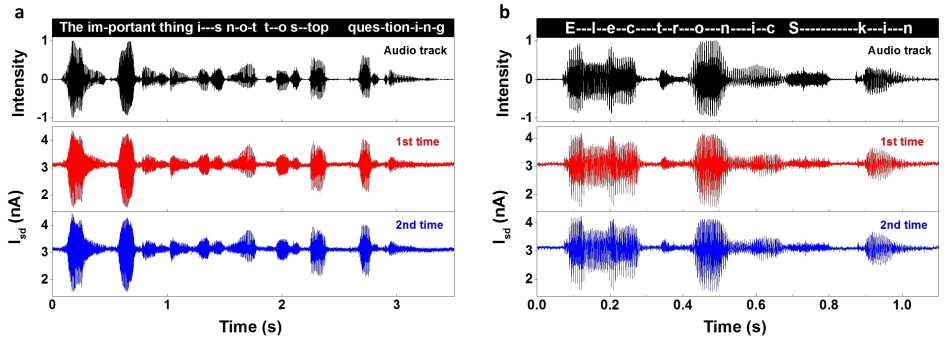

Figure 5-10 | Speech pattern recognition. Comparisons of the acoustic waveforms measured by a standard microphone (top figure) and the CMAG-MoS_2 E-skin (two figures at the bottom), respectively. The source-drain current response of our device was measured twice at constant V_{sd} = 1 V, while a speaker was played a non-native female speaker saying **(a)** "The important thing is not to stop questioning" and **(b)** "Electronic skin" at 85 dB. All the measurements were carried out in our lab (noise background at ~ 62 dB).

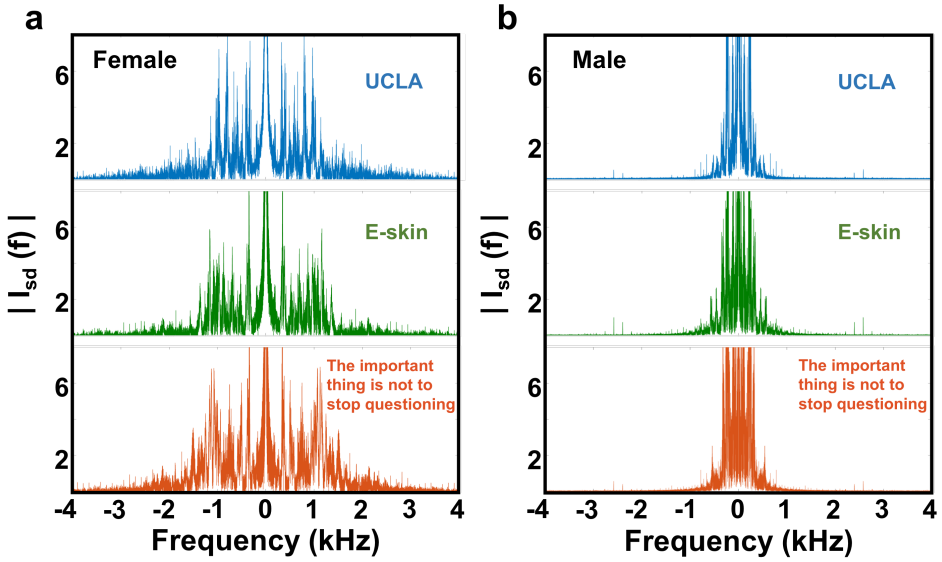

Figure 5-11 | E-skin microphone for speech pattern recognition to differentiate the gender of the speakers. Center Fourier transform signals showing the distinct sensing signals between **(a)** female and **(b)** male speakers saying "U-C-L-A" (top), "E-skin" (middle), and "The important thing is not to stop questioning" (bottom), respectively. The frequency domain signals show distinct frequency regime for the male voice (primarily in the low frequency range 0–1,000 Hz) and the female voice (in wide frequency range 0–2,000 Hz), independent off the exact words, allowing to differentiate the gender of the speakers.

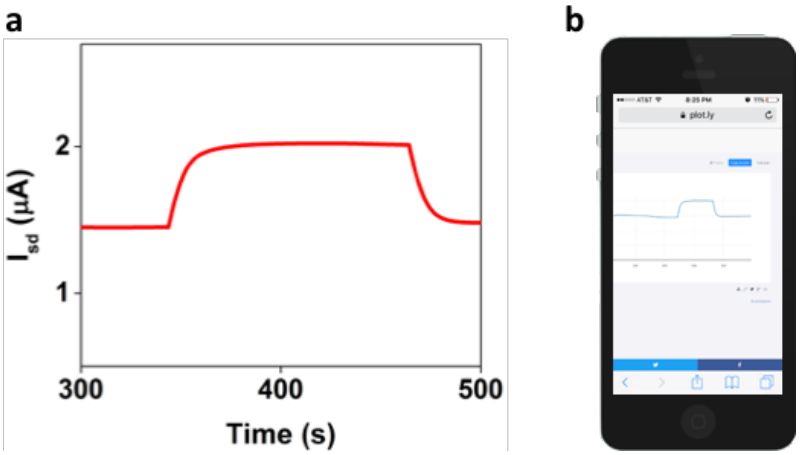

Figure 5-12 | Remote pressure monitoring. Integration of our CMAG-MoS_2 E-skin with system on chip (SoC) enables portable real-time remote pressure monitoring. **(a)** Source-drain current response to the applied pressure when our finger touched the device. **(b)** The real-time remote pressure monitoring can be assessed through the user's cell phone by using the open on-line website. The results can be sent to Facebook or Twitter.

References

1 Guo, C., Yu, Y. & Liu, J. Rapidly patterning conductive components on skin substrates as physiological testing devices via liquid metal spraying and pre-designed mask. *Journal of Materials Chemistry B* **2**, 5739-5745 (2014).

2 Hattori, Y. *et al.* Multifunctional skin-like electronics for quantitative, clinical monitoring of cutaneous wound healing. *Advanced healthcare materials* **3**, 1597-1607 (2014).

3 Honda, W., Harada, S., Arie, T., Akita, S. & Takei, K. Wearable, Human-Interactive, Health-Monitoring, Wireless Devices Fabricated by Macroscale Printing Techniques. *Advanced Functional Materials* **24**, 3299-3304 (2014).

4 Kaltenbrunner, M. *et al.* An ultra-lightweight design for imperceptible plastic electronics. *Nature* **499**, 458 (2013).

5 Mannsfeld, S. C. *et al.* Highly sensitive flexible pressure sensors with microstructured rubber dielectric layers. *Nature materials* **9**, 859 (2010).

6 Melzer, M. *et al.* Imperceptible magnetoelectronics. *Nature communications* **6**, 6080 (2015).

7 Pan, C. *et al.* High-resolution electroluminescent imaging of pressure distribution using a piezoelectric nanowire LED array. *Nature Photonics* **7**, 752 (2013).

8 Pan, L. *et al.* An ultra-sensitive resistive pressure sensor based on hollow-sphere microstructure induced elasticity in conducting polymer film. *Nature communications* **5**, 3002 (2014).

9 Pang, C. *et al.* A flexible and highly sensitive strain-gauge sensor using reversible interlocking of nanofibres. *Nature materials* **11**, 795 (2012).

10 Reeder, J. *et al.* Mechanically adaptive organic transistors for implantable electronics. *Advanced Materials* **26**, 4967-4973 (2014).

11 Sekitani, T. & Someya, T. Stretchable organic integrated circuits for large-area electronic skin surfaces. *Mrs Bulletin* **37**, 236-245 (2012).

12 Sekitani, T., Zschieschang, U., Klauk, H. & Someya, T. Flexible organic transistors and circuits with extreme bending stability. *Nature materials* **9**, 1015 (2010).

13 Takei, K. *et al.* Highly sensitive electronic whiskers based on patterned carbon nanotube and silver nanoparticle composite films. *Proceedings of the National Academy of Sciences* **111**, 1703-1707 (2014).

14 Tee, B. C., Wang, C., Allen, R. & Bao, Z. An electrically and mechanically self-healing composite with pressure-and flexion-sensitive properties for electronic skin applications. *Nature nanotechnology* **7**, 825 (2012).

15 Wang, C. *et al.* User-interactive electronic skin for instantaneous pressure visualization. *Nature materials* **12**, 899 (2013).

16 Wang, X. *et al.* Dynamic pressure mapping of personalized handwriting by a flexible sensor matrix based on the mechanoluminescence process. *Advanced Materials* **27**, 2324-2331 (2015).

17 Xu, S. *et al.* Stretchable batteries with self-similar serpentine interconnects and integrated wireless recharging systems. *Nature communications* **4**, 1543 (2013).

18 Yamada, T. *et al.* A stretchable carbon nanotube strain sensor for human-motion detection. *Nature nanotechnology* **6**, 296 (2011).

19 Zang, Y. *et al.* Flexible suspended gate organic thin-film transistors for ultra-sensitive pressure detection. *Nature communications* **6**, 6269 (2015).

20 Zhu, G. *et al.* Self-powered, ultrasensitive, flexible tactile sensors based on contact electrification. *Nano letters* **14**, 3208-3213 (2014).

21 Wang, X. *et al.* Recent progress in electronic skin. *Advanced Science* **2** (2015).

22 Kang, D. *et al.* Ultrasensitive mechanical crack-based sensor inspired by the spider sensory system. *Nature* **516**, 222-226 (2014).

23 Kim, D.-H. *et al.* Epidermal electronics. *Science* **333**, 838-843 (2011).

24 Lipomi, D. J. *et al.* Skin-like pressure and strain sensors based on transparent elastic films of carbon nanotubes. *Nature nanotechnology* **6**, 788-792 (2011).

25 Tee, B. C.-K. *et al.* A skin-inspired organic digital mechanoreceptor. *Science* **350**, 313-316 (2015).

26 Yeom, C. *et al.* Large-Area Compliant Tactile Sensors Using Printed Carbon Nanotube Active-Matrix Backplanes. *Adv. Mater.* **27**, 1561-1566 (2015).

27 Schwartz, G. *et al.* Flexible polymer transistors with high pressure sensitivity for application in electronic skin and health monitoring. *Nat. Commun.* **4**, 1859 (2013).

28 Lee, S. *et al.* A transparent bending-insensitive pressure sensor. *Nat Nanotechnol* **11**, 472-478 (2016).

29 Graz, I. *et al.* Flexible ferroelectret field-effect transistor for large-area sensor skins and microphones. *Applied physics letters* **89**, 073501 (2006).

30 Takahashi, T., Takei, K., Gillies, A. G., Fearing, R. S. & Javey, A. Carbon nanotube active-matrix backplanes for conformal electronics and sensors. *Nano Lett.* **11**, 5408-5413 (2011).

31 Mendis, S., Puska, P. & Norrving, B. *Global atlas on cardiovascular disease prevention and control*. (World Health Organization, 2011).

32 Nichols, W. W. Clinical measurement of arterial stiffness obtained from noninvasive pressure waveforms. *Am. J. Hypertens.* **18**, 3S-10S (2005).

33 Millasseau, S., Kelly, R., Ritter, J. & Chowienczyk, P. Determination of age-related increases in large artery stiffness by digital pulse contour analysis. *Clin. Sci.* **103**, 371-377 (2002).

34 Munir, S. *et al.* Exercise reduces arterial pressure augmentation through vasodilation of muscular arteries in humans. *Am. J. Physiol. Heart Circ. Physiol.* **294**, H1645-H1650 (2008).

35 Flanagan, J. L. *Speech analysis synthesis and perception*. Vol. 3 (Springer Science & Business Media, 2013).

36 Saunders, F. A., Hill, W. A. & Franklin, B. A wearable tactile sensory aid for profoundly deaf children. *J. Med. Syst.* **5**, 265-270 (1981).

37 Yang, J. *et al.* Eardrum-Inspired Active Sensors for Self-Powered Cardiovascular System Characterization and Throat-Attached Anti-Interference Voice Recognition. *Adv. Mater.* **27**, 1316-1326 (2015).

Chapter 6: Conclusion and future perspectives

With a unique design of the CMAGs, our E-skins are able to overcome the challenges of current pressure sensitive E-skins, lower pressure sensitivity and slower response, at the same time. The conecpt of CMAGs can create capacitor- or transistor-based E-skins for pressure sensing. The capacitor-based E-skins by integrating with CMAGs show highest sensitivity up to 770.4 kPa^{-1} (*vs.* ~ 4.5 kPa^{-1} reported previously). Moreover, by employing the CMAGs as pressure sensitive gate, our CMAG-2D semiconductor E-skins achieve record-high sensitivty ~ 2.61×10^7 kPa^{-1} (*vs.* the previous record of 192 kPa^{-1}), ultrafast response (< 0.1 ms *vs.* 10 ms reported previosuly), lower power consumption (~ 9 pW−270 nW), low minimum pressure detection (< 0.05 Pa *vs.* ~ 0.5 Pa reported before) and excellent stability, which deliver an overall performance well above the existing pressure sensing E-skins. Furthermore, we demonstrated the applications of CMAG E-skins in highly sensitive static pressure mapping, real-time human pulse wave measurements, E-skin microphone for speech pattern recognition, and remote pressure monitoring, which might pave a way for next generation of flexible electronics and related applications.

In the future, we may optomize the pressure sensing performance of our CMAG E-skins by using multiple sizes of the conductive pyramids or other conductive microstructures to futher enhance the pressure sensitivity and broaden the pressure sensing range. By using the stretchable elastomers embeded with the codnuctive fillets (*i.e.*, CNTs, conductive particles, 3D graphene foams, *etc*.), the stretchable and conformal CMAG E-skins can be realized for the applications in soft robotics and stretchable electronic devices. In addition, integrating different kinds of sensors and electronic devices (*i.e.*, temeprature sensors, magnetic sensors, LEDs, *etc.*) with our CMAG E-skins can realize multifuctional E-skins for healthcare monitoring, human-machine interface,

artificial intelligence and related applications. With the integration of the speakers, we may not only turn CMAG E-skin arrays to the microphone but also to the speaker, which might be the exciting applications for futhre touch panels and devices.